the ρ-mass region (see Ref. 8).
[8]G. Grayer *et al.*, Nucl. Phys. B50, 29 (1972).
[9]C. Michael, in Springer Tracts in Modern Physics, edited by G. Höhler (Springer, New York, 1970), Vol. 55, p. 174.
[10]P. Estabrooks and A. D. Martin, Phys. Lett. 41B, 350 (1972).
[11]P. Estabrooks *et al.*, in π-π *Scattering—1973*, proceedings of the international conference on π-π scattering and associated topics, Tallahassee, 1973, edited by P. K. Williams and V. Hagopian (A.I.P., New York, 1973), p. 37.
[12]The parametric forms were chosen to accommodate the various exchange contributions; for instance, each $\lambda_t = 0$ amplitude included a (π-exchange) term $g\sqrt{-t}\exp(bt)/(\mu^2 - t)$. Further, the parameterization allowed the possibility of A_2-exchange, nonevasive contributions to the $\lambda_s \neq 0$ amplitudes and $\lambda_t \neq 0$ pion-exchange contributions.
[13]P. Estabrooks, A. D. Martin, and C. Michael, CERN Report No. TH-1732, 1973 (unpublished).
[14]P. K. Williams, Phys. Rev. D 1, 1312 (1970).
[15]An example of this approach is the Williams model (Ref. 14).
[16]A. D. Martin, in *Proceedings of the IV International Symposium on Multiparticle Hadrodynamics, Pavia, 1973*, edited by F. Duimio *et al.* (Istituto Nazionale di Fisica Nucleare, 1973), p. 203.
[17]C. Schmid, Phys. Rev. Lett. 20, 628 (1968).
[18]V. Barger and R. J. N. Phillips, Nucl. Phys. B32, 93 (1971).
[19]See, e.g., K. Gottfried and J. D. Jackson, Nuovo Cimento 34, 735 (1965).

PHYSICAL REVIEW D VOLUME 10, NUMBER 1 1 JULY 1974

Charge-exchange vector-meson production*

R. D. Field†
Brookhaven National Laboratory, Upton, New York 11973

Deepinder P. Sidhu‡
Institute for Theoretical Physics, State University of New York at Stony Brook, Stony Brook, New York 11790
(Received 4 September 1973)

We present an analysis of the six charge-exchange vector-meson production reactions $\pi^- p \to \rho^0 n$, $\pi^+ n \to \rho^0 p$, $\pi^- p \to \omega^0 n$, $\pi^+ n \to \omega^0 p$, $K^- p \to \bar{K}^{*0} n$, and $K^+ n \to K^{*0} p$ using Regge-pole plus absorption models and SU(3). Our aim is to understand what existing data imply about these models and to predict and discuss the behavior of as-yet-unmeasured observables. We discuss in detail the amounts of s-channel helicity-nonflip, -flip, and -double-flip absorption required to fit the data. Such topics as the line-reversal breaking in K^{*0} and $\bar{K}^{*0}$ production, the status of the ρ wrong-signature nonsense zero in ω^0 production, and the nature of A_1 exchange are discussed. The electromagnetic mixing of the ρ^0 and ω^0 meson provides a powerful tool for probing the nature of strong-interaction production amplitudes, and examinations of the effects of ρ^0-ω^0 mixing on the $\pi^+\pi^-$ mass spectra and on isospin violations in ω^0 productions are included. We find that some of the new absorption models are capable of explaining many features in ρ^0 and ω^0 production and that one is able to predict correctly [using SU(3)] the observables for K^{*0} and $\bar{K}^{*0}$ production including the line-reversal breaking. The models have problems in predicting the correct energy dependences of $\rho^H_{00} d\sigma/dt$ and $\rho^H_+ d\sigma/dt$ for ρ^0 production, and have some difficulties in explaining the recent ρ-ω interference data at 4.0 GeV/c, which show a spike at the ω^0 mass of the observable $\rho^H_+ d\sigma/dt\, dm\,(\pi^- p \to (\pi^+\pi^-)n)$.

I. INTRODUCTION

In recent years our knowledge of the behavior of two-body production amplitudes has increased primarily because of the measurement of additional observables (P, A, R, $\rho^{mm'}_{nn'}$, etc.) which allows for model-independent amplitude analyses.[1] For example, from the Michael and Halzen[2] amplitude analysis of $\pi N \to \pi N$ we have learned that there are large absorptive corrections to the s-channel helicity-nonflip amplitude.[3] The situation as to absorption of the helicity-flip amplitude is not clear, however. Some authors[4] believe that the s-channel helicity-flip absorption is small or zero and that these amplitudes are described by pure poles with WSNZ (wrong-signature nonsense zeros), while others exclude WSNZ and absorb all amplitudes similarly.[5]

In cases where a model-independent analysis is not possible, it is necessary to resort to model fitting. One can then examine the resulting amplitude structure. This is somewhat inferior to a

model-independent analysis since the model-determined amplitudes are not unique. Nevertheless one can, by studying a set of reactions simultaneously, place great restrictions on such models. One such set of reactions is the six charge-exchange vector-meson production reactions[6]

$$\pi^- p \to \rho^0 n, \tag{1.1}$$

$$\pi^+ n \to \rho^0 p, \tag{1.2}$$

$$\pi^- p \to \omega^0 n, \tag{1.3}$$

$$\pi^+ n \to \omega^0 p, \tag{1.4}$$

$$K^- p \to \bar{K}^{*0} n, \tag{1.5}$$

$$K^+ n \to K^{*0} p. \tag{1.6}$$

The reactions $\pi N \to \omega^0 N$ and $\pi N \to \rho^0 N$ are related to the reactions $\bar{K}N \to \bar{K}^{*0}N$ by SU(3). Given the amplitudes for ω^0 and ρ^0 production one can predict the amplitudes for $\bar{K}^{*0}$ production. In fact if one is willing to neglect absorption and assume exchange-degenerate (EXD) trajectories for the π and B, and for the ρ and A_2 [i.e., $\alpha_\pi(t) = \alpha_B(t)$, $\alpha_{A_2}(t) = \alpha_\rho(t)$], then one can use SU(3) to relate directly the observables for ω^0, ρ^0, and $\bar{K}^{*0}$ production as follows:

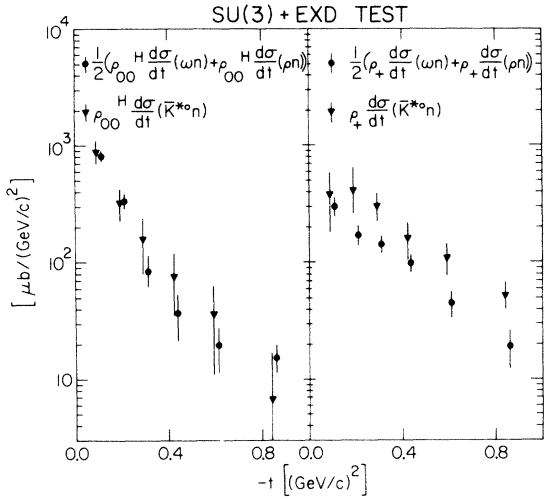

FIG. 1. SU(3) plus EXD test. Assuming no absorption and weak EXD [$\alpha_{A_2}(t) = \alpha_\rho(t)$, $\alpha_\pi(t) = \alpha_B(t)$], SU(3) implies

$$\frac{1}{2}\left[\rho_{00}^H \frac{d\sigma}{dt}(\pi^- p \to \omega^0 n) + \rho_{00}^H \frac{d\sigma}{dt}(\pi^- p \to \rho^0 n)\right] = \rho_{00}^H \frac{d\sigma}{dt}(K^- p \to \bar{K}^{*0} n)$$

and

$$\frac{1}{2}\left[\rho_\pm^H \frac{d\sigma}{dt}(\pi^- p \to \omega^0 n) + \rho_\pm^H \frac{d\sigma}{dt}(\pi^- p \to \rho^0 n)\right] = \rho_\pm^H \frac{d\sigma}{dt}(K^- p \to K^{*0} n),$$

where $\rho_\pm^H = \rho_{11}^H \pm \rho_{1-1}^H$.

$$\frac{1}{2}\left[\rho_{00}^H \frac{d\sigma}{dt}(\omega^0 n) + \rho_{00}^H \frac{d\sigma}{dt}(\rho^0 n)\right] = \rho_{00}^H \frac{d\sigma}{dt}(\bar{K}^{*0} n), \tag{1.7a}$$

$$\frac{1}{2}\left[\rho_\pm^H \frac{d\sigma}{dt}(\omega^0 n) + \rho_\pm^H \frac{d\sigma}{dt}(\rho^0 n)\right] = \rho_\pm^H \frac{d\sigma}{dt}(\bar{K}^{*0} n), \tag{1.7b}$$

where $\rho_\pm^H = \rho_{11}^H \pm \rho_{1-1}^H$. Such a comparison is shown in Fig. 1.[7] We see that the agreement is quite good for $\rho_{00}^H d\sigma/dt$ and not so good for $\rho_+^H d\sigma/dt$. We will examine in detail how absorption effects modify these naive predictions.

In this paper we present an analysis of the above six charge-exchange vector-meson production reactions using Regge-pole plus absorption models and SU(3). We do not intend to confront the reader with a mammoth χ^2-fitting exercise. We fit only the $\pi^- p \to \omega^0 n$ data at 4.5 GeV/c and the $\pi^- p \to \rho^0 n$ data at 4.42 GeV/c. The observables at other energies and for other reactions are then predicted. Our aim is to understand what the data imply about Regge-pole plus absorption models and to see how well SU(3) works in relating ω^0 and ρ^0 production to $\bar{K}^{*0}$ production. In addition to knowledge gained by studying the vector-meson density-matrix elements, the electromagnetic mixing of the ρ^0 and ω^0 mesons places great restrictions on the relative ρ^0 and ω^0 production amplitudes. ρ-ω mixing effects are, for this reason, studied in great detail.

The paper is divided into three sections. In Sec. II we confront the models with the data. This section is arranged as follows:

II. The models versus the data
- A. Reaction $\pi^- p \to \rho^0 n$
  1. Models 1 and 2: Fitting procedure
  2. Behavior of $\rho_{11}^H d\sigma/dt(\pi^- p \to \rho^0 n)$ and $n = 0$ (nonflip) absorption
  3. Behavior of $\mathrm{Re}\rho_{10}^H(\pi^- p \to \rho^0 n)$ and $n = 0$ absorption
  4. Behavior of $\rho_{00}^H d\sigma/dt(\pi^- p \to \rho^0 n)$ and $n = 1$ absorption
  5. Alternative explanation of the behavior of $\rho_{00}^H d\sigma/dt(\pi^- p \to \rho^0 n)$ (model 3): Tests for A_1 exchange
  6. Behavior of $\rho_+^H(\pi^- p \to \rho^0 n)$: A_2 pole versus π cut
  7. Energy dependences: Possible trouble spot
- B. Reactions $\pi^- p \to \omega^0 n$ and $\pi^+ n \to \omega^0 p$
  1. Models 1a, 1b, and 2: Fitting procedure
  2. Behavior of $\rho_+^H(\pi N \to \omega^0 N)$: ρ pole versus B cut
  3. Behavior of $\rho_{00}^H d\sigma/dt(\pi N \to \omega^0 N)$: Where do helicity-zero ω^0's come from?
  4. Isospin violations due to ρ-ω mixing

5. Unmeasured observables
C. π-π mass spectra: ρ-ω interference
D. Reactions $K^-p \to \bar{K}^{*0}n$ and $K^+n \to K^{*0}p$
1. SU(3) predictions
2. Line-reversal behavior
3. Unmeasured observables: A_1 exchange?

We reserve Sec. III for summary and conclusions.

II. THE MODELS VERSUS THE DATA

A. Reaction $\pi^-p \to \rho^0 n$

1. *Models 1 and 2: Fitting procedure*

We fit the differential cross section and vector-meson density-matrix elements for the reaction $\pi^-p \to \rho^0 n$ at 4.42 GeV/c using the following Regge-pole plus absorption models:

(a) Model 1. For this model we use the prescriptions of Hartley and Kane.[5] This model includes non-EXD input Regge poles with $\alpha_{A_2}(t) = 0.3 + 1.0t$ and $\alpha_\pi(t) = 0.5(t - m_\pi{}^2)$, which are absorbed with an effective scattering amplitude (see Fig. 2) given by

$$T_{\text{eff}}(s,t) = P(s,t) + D_0(s,t), \tag{2.1}$$

where $P(s,t)$ is the s-channel helicity-conserving "Pomeron" amplitude and $D_0(s,t)$ is the helicity-nonflip contribution from diffractive dissociation. The parametrizations of $P(s,t)$ and $D_0(s,t)$ used are identical to those used by Hartley and Kane[5] to describe pseudoscalar production except for the strength of $D_0(s,t)$, which was increased by a factor of ≈ 1.5.[8] This increased absorption was necessary to explain the large absorption effects seen in vector-meson production. Figure 3 shows the effective partial-wave absorbing function $f^j_{\text{eff}}(s)$ resulting from this model.[9]

Model 1 contains no A_1 contribution. In addition all fits resulted in $\gamma^{A_2}_{++} \approx 0$.[10] This is no doubt an approximation since evidence from pseudoscalar production gives a ratio $\gamma^{A_2}_{+-}/\gamma^{A_2}_{++}$ of from 3 to 10. Including a small A_2-nucleon helicity-nonflip coupling does not alter any of the conclusions except those concerning polarizations resulting from

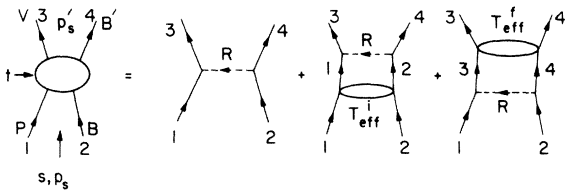

FIG. 2. Illustrates that the total scattering amplitude for $PB \to VB'$ is given by the sum of t-channel Regge exchanges (R) plus absorptive corrections. The quantities $T^{i,f}_{\text{eff}}$ are the initial- (final-) state effective scattering amplitudes.

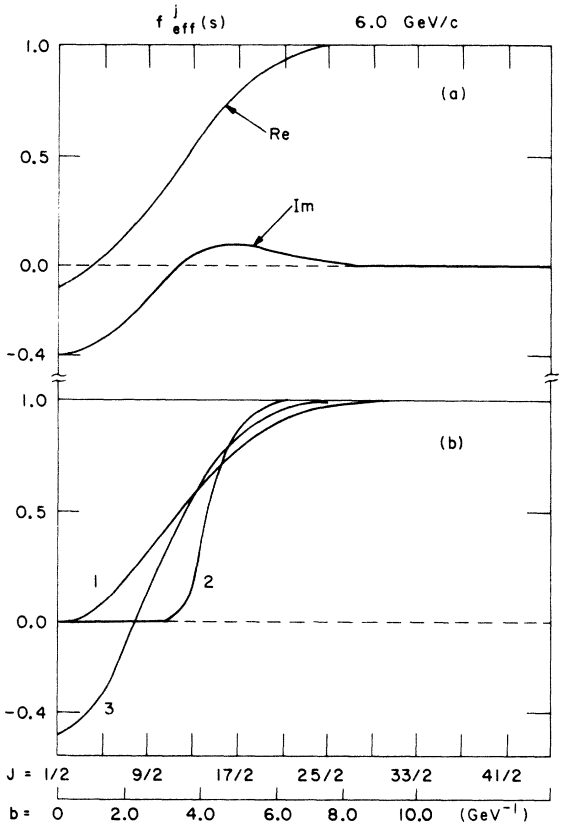

FIG. 3. The effective partial-wave absorption factor $f^j_{\text{eff}}(s)$ at 6.0 GeV/c for (a) model 1 absorption (fancy Pomeron absorption model); (b) curve 1 is the absorption factor for complete S-wave absorption; curve 2 is square-cut absorption, curve 3 is the same as curve 2 but with an arbitrary λ factor multiplying the strength ($\lambda = 1.5$).

natural-parity exchange.

Figure 4 shows the resulting fit to the differential cross section and Fig. 5 the fit to the density-matrix elements for the reaction $\pi^-p \to \rho^0 n$ at 4.42 GeV/c. Having determined the Regge residues and absorption parameters by fitting the 4.42-GeV/c $\pi^-p \to \rho^0 n$ data, we then predict observables at other energies. In Fig. 4 we show the predicted differential cross section for $\pi^-p \to \rho^0 n$ at 6.0 and 15.0 GeV/c, and in Fig. 5 show the predicted vector-meson density-matrix elements at 6.0 GeV/c.

We are particularly interested in the detailed behavior of the s-channel helicity amplitudes resulting from this model. The magnitudes and phases of these amplitudes for the reaction $\pi^-p \to \rho^0 n$ at 6.0 GeV/c are shown in Fig. 6 as a function of t for $0 \leq |t| \leq 1.0$ (GeV/c)^2. In Fig. 7 we present Argand diagrams of the contributions to the s-channel helicity amplitudes for $\pi^-p \to \rho^0 n$ at 4.0 GeV/c and with $t - t_0 = -0.1$ (GeV/c)^2.

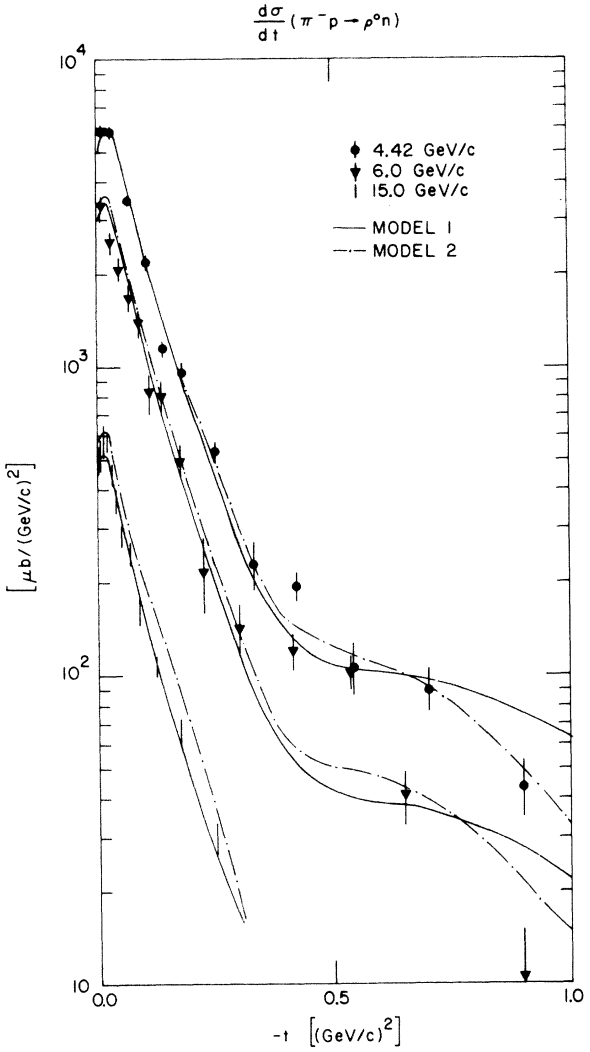

FIG. 4. Shows a comparison of model 1 (fancy Pomeron absorption) and model 2 (square-cut absorption) with the data on the differential cross section for $\pi^- p \to \rho^0 n$ at 4.42 (Ref. 30), 6.0 (Ref. 31), and 15.0 GeV/c (Ref. 32).

(b) Model 2. For this model we use the "square-cut" type of absorption introduced by Worden[11] in fitting photoproduction. We generalize this model a bit to allow for different absorption for each net helicity-flip amplitude. This model has very large (square-cut) type of absorption for the $n=0$ (helicity-nonflip) amplitudes [curve 2, Fig. 3(b)]. It has less absorption for $n=1$ (single flip) amplitudes; however, the absorption is still quite large and is strong enough to completely absorb the s wave [curve 1, Fig. 3(b)]. This model does not absorb $n=2$ (double flip) amplitudes. The π and A_2 trajectories are taken to be $\alpha_\pi(t)=0.5(t-m_\pi{}^2)$ and $\alpha_{A_2}(t)=0.5+t$, respectively.

We tried using the same "square-cut" absorption [curve 2, Fig. 3(b)] for each helicity amplitude, but this large absorption when applied to the $n=1$ amplitude $H^{\eta=1}_{0-;+}$ caused the observable $\rho^H_{00}d\sigma/dt(\pi^- p \to \rho^0 n)$ to have a dramatic dip at small $|t|$ values similar to that shown in Fig. 8 ($\lambda=1.25$). We concluded that the very strong "square-cut" absorption should apply only to $n=0$ amplitudes and reduced the $n=1$ absorption to the size shown by curve 1 in Fig. 3(b). Assuming no A_1 exchange, it is necessary to absorb $n=1$ amplitudes in order to fit the large-$|t|$ behavior of $\rho^H_{00}d\sigma/dt(\pi^- p \to \rho^0 n)$ (see Sec. II A 4). We fit only the 4.42-GeV/c $\pi^- p \to \rho^0 n$ data and predict the observables at other energies. In Fig. 4 we compare this model with the differential cross sections for $\pi^- p \to \rho^0 n$ at 4.42, 6.0, and 15.0 GeV/c and in Fig. 5 with the vector-meson density-matrix elements at 4.42 and 6.0 GeV/c.

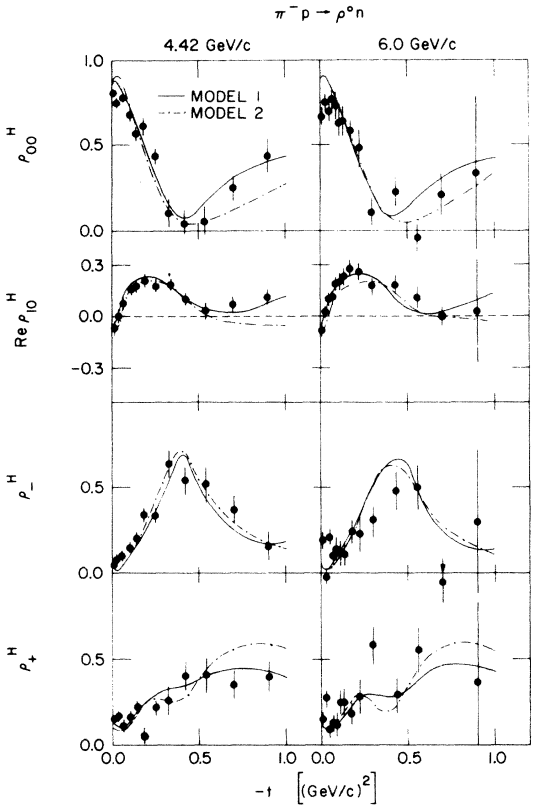

FIG. 5. Shows a comparison of model 1 (fancy Pomeron absorption) and model 2 (square-cut absorption) with the data on the vector-meson density-matrix elements for $\pi^- p \to \rho^0 n$ at 4.42 (Ref. 30) and 6.0 GeV/c (Ref. 31).

2. *Behavior of $\rho^H_{11}d\sigma/dt(\pi^- p \to \rho^0 n)$ and $n=0$ (nonflip) absorption*

It is a well-known result that the Regge-pole contributions to the observable

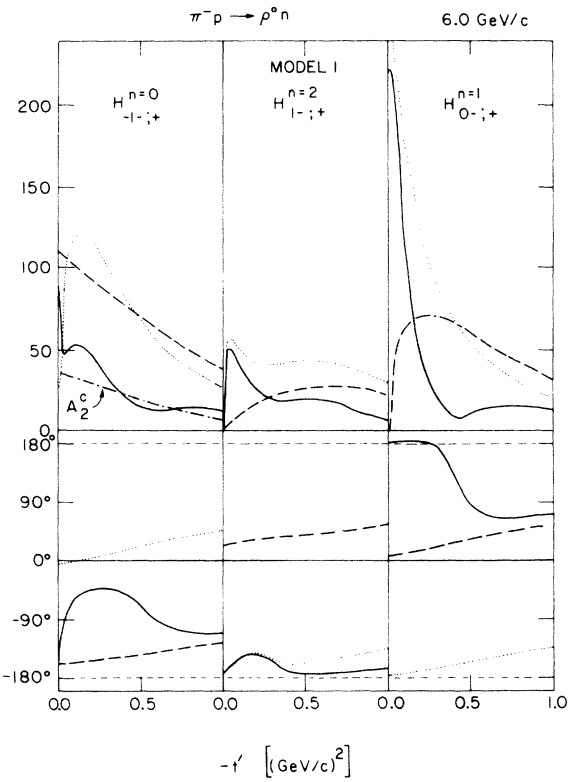

FIG. 6. Magnitudes (upper curves) and phases (lower curves) of the s-channel helicity amplitudes for model 1 (fancy Pomeron absorption) at 6.0 GeV/c. The solid, dotted, and dashed curves correspond to the total, Regge-pole, and Regge-cut contributions, respectively. The A_2-cut contribution to the evasive $n = 0$ amplitude $H^{n=0}_{-1-;+}$ is also shown.

$$\rho^H_{11}\frac{d\sigma}{dt} = 2K(|H^{n=0}_{-1-;+}|^2 + |H^{n=1}_{1+;+}|^2 + |H^{n=1}_{-1+;+}|^2 + |H^{n=2}_{1-;+}|^2) \qquad (2.2)$$

produce a dip in the forward direction even though this is not required by angular momentum conservation.[12] This is because the (evasive) Regge-pole contributions to $H^{n=0}_{-1-;+}$ vanishes at $t=0$. The Regge-cut contribution to this $n=0$ amplitude need not vanish at $t=0$ (or $t=t_0$) (see Fig. 6), and thus with large $n=0$ absorption the quantity $\rho^H_{11}d\sigma/dt$ is no longer expected to dip in the forward direction.[13] This observable is thus an excellent measure of the strength of the $n=0$ absorption: A dip at small $|t|$ implies small absorption; a spike implies large absorption.

In Fig. 9 we compare the experimentally determined small-$|t|$ behavior of $\rho^H_{11}d\sigma/dt(\pi^- p \to \rho^0 n)$ with models 1 and 2 at 4.42, 6.0, and 15.0 GeV/c. The data at 6.0 and 15.0 GeV/c show a definite spike in the forward direction, indicating large

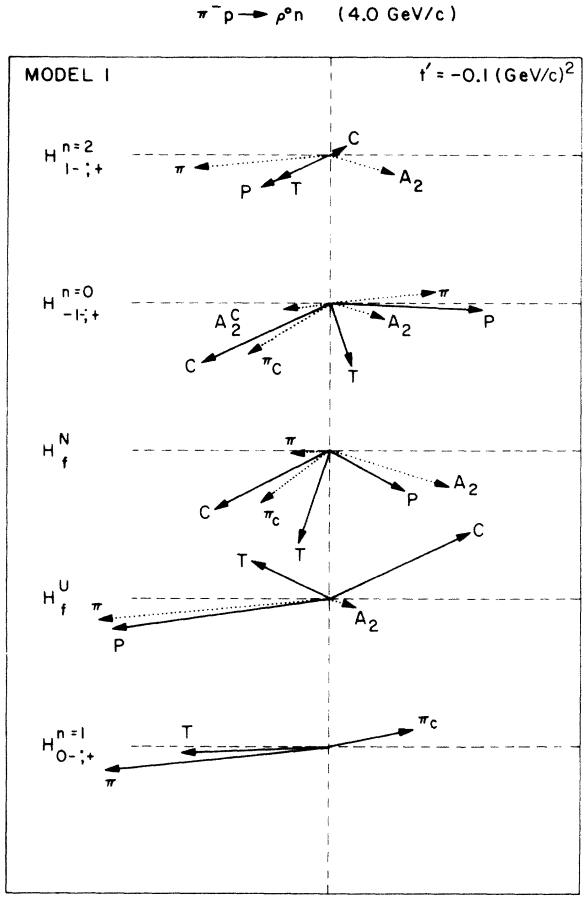

FIG. 7. Argand diagram of the various contributions to the s-channel helicity amplitudes at $t' \equiv t - t_0 = -0.1$ (GeV/c)^2 from model 1 (fancy Pomeron absorption). The labels P and C correspond to the total pole ($\pi + A_2$) and total cut ($\pi_C + A_2^C$) contributions, respectively. The resulting total amplitude (pole + cut) is labeled T. The amplitudes H^N_f and H^U_f are defined in (2.8).

$n=0$ absorption. Figure 10 shows various contributions to $\rho^H_{11}d\sigma/dt(\pi^- p \to \rho^0 n)$ from model 1 at 6.0 GeV/c. The π and A_2 pole contributions show a marked dip in the forward direction. The forward spike is produced by the sum of the π and A_2 cuts. From Fig. 6 it can be seen that the A_2 cut makes up $\approx$34% of the amplitude $H^{n=0}_{-1-;+}$ in the forward direction. The remaining 76% is the π cut. In order to produce the observed peaking in $\rho^H_{11}d\sigma/dt$ it is necessary that the π and A_2 cuts interfere constructively in $H^{n=0}_{-1-;+}$. This requires that the relative π-A_2 pole phase be such that the real parts of the π and A_2 poles have the same sign in $H^{n=0}_{-1-;+}$ (see Fig. 7). Since the π-pole (and thus also π-cut) contribution changes sign in going from $H^{n=0}_{-1-;+}$ to $H^{n=2}_{1-;+}$, the π and A_2 cuts interfere destructively in the $n=2$ amplitude (see Fig. 7) resulting in small $n=2$ absorption.

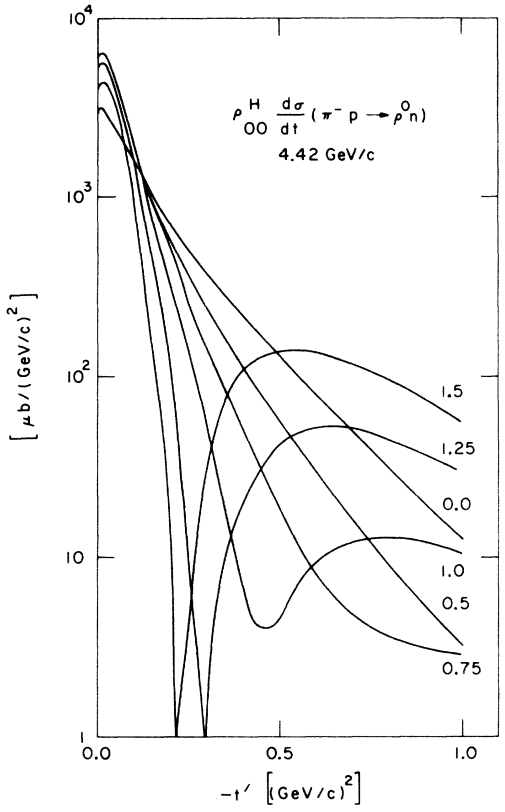

FIG. 8. Fits to $\rho_{00}^H d\sigma/dt$ $(\pi^- p \to \rho^0 n)$ at 4.42 GeV/c using a model with varying degrees of $n = 1$ (single flip) absorption, where $\lambda_{n=1} = 0.0$ (no absorption), 0.5, 0.75, 1.0, 1.25, 1.5.

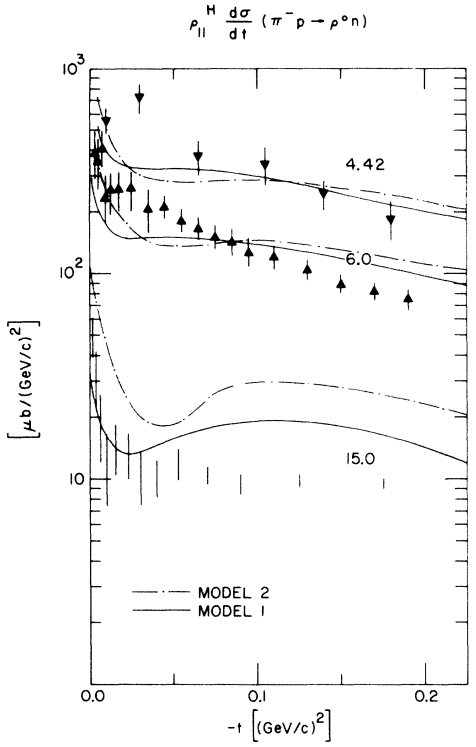

FIG. 9. A comparison of model 1 (fancy Pomeron absorption) and model 2 (square-cut absorption) with the data on the small-$|t|$ behavior of $\rho_{11}^H d\sigma/dt$ $(\pi^- p \to \rho^0 n)$ at 4.42 (Ref. 30), 6.0 (Ref. 33), and 15.0 (Ref. 32).

3. *Behavior of* $\mathrm{Re}\rho_{10}^H(\pi^- p \to \rho^0 n)$ *and* $n = 0$ *absorption*

The large $n = 0$ (nonflip) absorption necessary to fit the experimental data on $\rho_{11}^H d\sigma/dt(\pi^- p \to \rho^0 n)$ produces an interesting effect on the small-$|t|$ behavior of $\mathrm{Re}\rho_{10}^H$. In the absence of A_1 exchange

$$\mathrm{Re}\rho_{10}^H \frac{d\sigma}{dt} = -K\,\mathrm{Re}(H_f^U H_{0-;+}^{*}) = +K|H_f^U||H_{0-;+}^{n=1}|\cos\varphi\,, \tag{2.3}$$

where

$$\varphi = \arg H_{0-;+}^{n=1} - \arg H_f^U\,, \tag{2.4}$$

and where

$$H_f^U = H_{1-;+}^{n=2} - H_{-1-;+}^{n=0}.$$

In the absence of absorption the π Regge-pole contributions to H_f^U and $H_{0-;+}^{n=1}$ have the same phase given by the Regge signature factor and thus $\mathrm{Re}\rho_{10}^H$ is structureless (dotted curve in Fig. 11). In the presence of absorption, however, the small-$|t|$ phase of $H_{-1-;+}^{n=0}$ is drastically changed. Very near the forward direction $H_{-1-;+}^{n=0}$ is given completely by Regge-cut contributions which are roughly 180° out of phase with the π pole (see Fig. 6). Then as $|t|$ increases the relative amount of π pole increases markedly causing the phase to change and become more like that of the π pole. The result of this is that the phase of $H_{-1-;+}^{n=0}$ changes from $\approx -160°$ in the forward direction to $\approx -45°$ at $t' = -0.2$ $(\mathrm{GeV}/c)^2$. At the same time the phase of the amplitude $H_{0-;+}^{n=1}$ is smooth and roughly that of the π pole ($\approx -180°$). Because of the rapid change of phase of $H_{-1-;+}^{n=0}$ and the smooth behavior of $H_{0-;+}^{n=1}$ the relative phase φ changes rapidly for small $|t|$ and goes through $\pm 90°$ for $|t| = 0.01 - 0.03$ $(\mathrm{GeV}/c)^2$. This causes $\mathrm{Re}\rho_{10}^H$ to change sign at small $|t|$ (see Fig. 11).[14] It is interesting that this $|t|$ behavior of $\mathrm{Re}\rho_{10}^H$ is a direct result of the peaking of $\rho_{11}^H d\sigma/dt$.

4. *Behavior of* $\rho_{00}^H d\sigma/dt(\pi^- p \to \rho^0 n)$ *and* $n = 1$ *absorption*

The question of the amount of $n = 1$ (helicity-flip) absorption has provided much controversy over the past years. For example, in the reaction $\pi^- p \to \pi^0 n$ the ρ couples predominantly to the $n = 1$ amplitude H_{+-}, and the data show a dip in the differ-

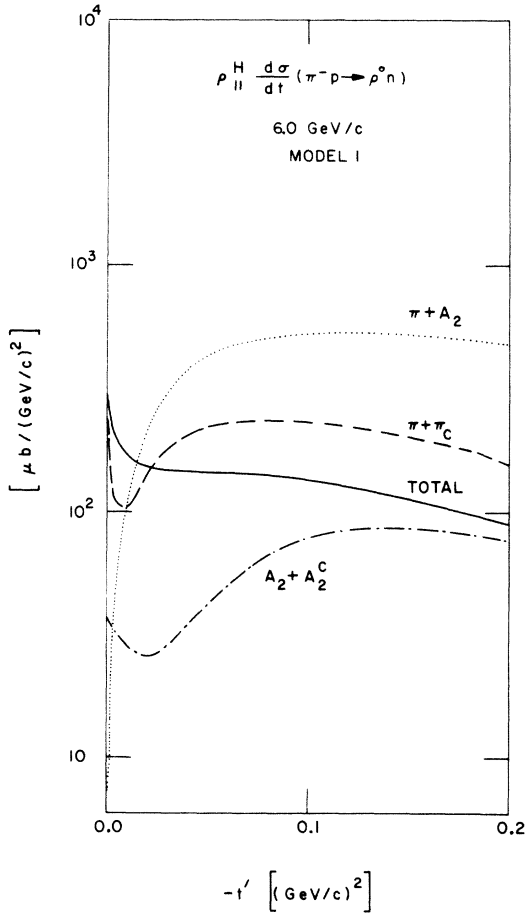

FIG. 10. Contributions to small-$|t|$ behavior of $\rho_{11}^H d\sigma/dt(\pi^- p \to \rho^0 n)$ at 6.0 GeV/c from model 1 (fancy Pomeron absorption).

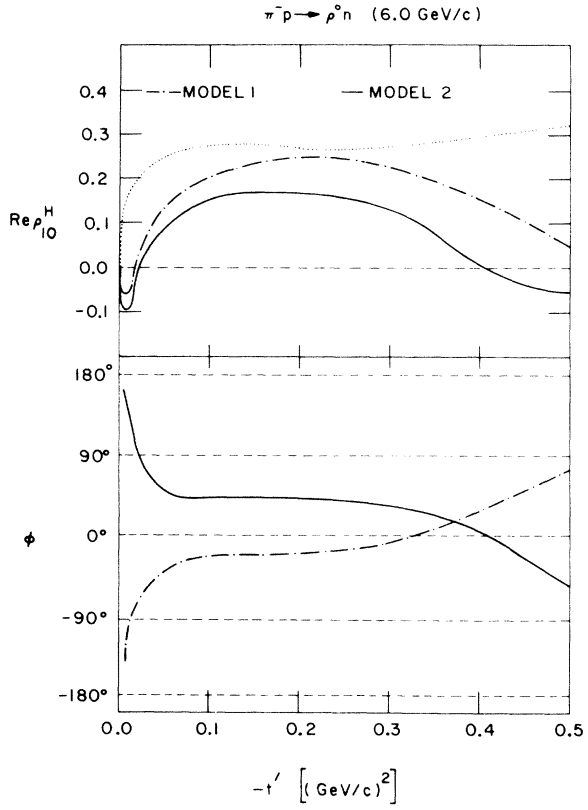

FIG. 11. Behavior of $\mathrm{Re}\rho_{10}^H$ and phase angle φ for $\pi^- p \to \rho^0 n$ at 6.0 GeV/c from model 1 (fancy Pomeron absorption) and model 2 (square-cut absorption). The dotted curve is model 2 before absorption effects are included. The phase φ is defined by $\varphi = \arg(H_{0-;+}^{n=1}) - \arg(H_f^U)$, where $H_f^U = H_{1-;+}^{n=2} - H_{-1-;+}^{n=0}$.

ential cross section at $t \approx -0.6$ (GeV/c)^2. Proponents of the weak-cut model believe that $n = 1$ absorption is small or zero and attribute the dip to a wrong-signature nonsense zero (WSNZ) of the ρ exchange amplitude. Proponents of the strong-cut model (SCRAM) or the new "fancy Pomeron absorption model" believe in large $n = 1$ absorption and produce dips via pole-cut interferences (no WSNZ). Both models predict dips in the $n = 1$ dominated differential cross section for $\pi^- p \to \pi^0 n$, and one has to resort to other more complicated ways of discriminating between the two models.[15]

Assuming no A_1 contribution (we will discuss the validity of this assumption later) the observable $\rho_{00}^H d\sigma/dt(\pi^- p \to \rho^0 n)$ is the square of the $n = 1$ amplitude $H_{0-;+}^{n=1}$ and receives contributions from π exchange and possibly an $n = 1$ π cut. The π Regge trajectory does not have a WSNZ at $t \approx -0.6$ (GeV/c)^2, and hence the two models mentioned above have different predictions for this observable. A model with sizable $n = 1$ absorption will predict a dip in $\rho_{00}^H d\sigma/dt(\pi^- p \to \rho^0 n)$, whereas a model with little or no $n = 1$ absorption will predict no dip. This is illustrated in Fig. 8, where we fit $\rho_{00}^H d\sigma/dt(\pi^- p \to \rho^0 n)$ at 4.42 GeV/c with a model consisting of a π pole plus varying amounts of $n = 1$ absorption. Pure π exchange produces a smooth structureless large-t behavior of $\rho_{00}^H d\sigma/dt$. As the absorption increases a dip appears and moves inward and the size of the rather flat large-$|t|$ bump depends on the amount of absorption. The larger the absorption the larger the bump after the dip.

In Fig. 12 we compare models 1 and 2 with $\rho_{00}^H d\sigma/dt(\pi^- p \to \rho^0 n)$ at 4.42, 6.0, 7.0, and 17.2 GeV/c. The data are somewhat inconclusive. The 4.42-, 6.0-, and 7.0-GeV/c bubble-chamber data show indications of a dip, whereas the high-statistics spark-chamber data at 6.0 and 17.2 GeV/c show a change in slope but no dip. Both models 1 and 2 have $n = 1$ absorption and thus predict dips. It is not possible (with no A_1 exchange)

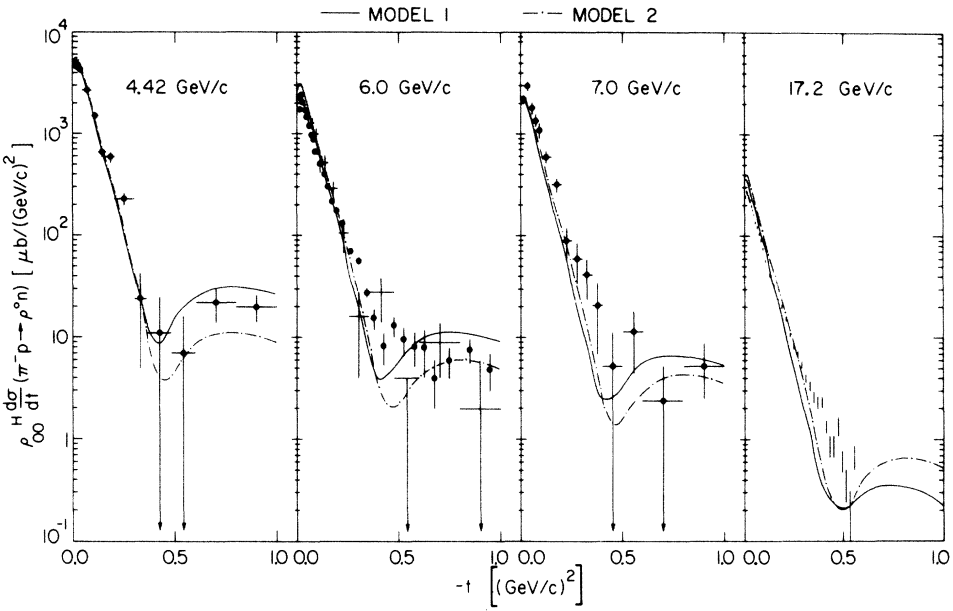

FIG. 12. Comparison of model 1 (fancy Pomeron absorption) and model 2 (square-cut absorption) with the data for $\rho_{00}^H d\sigma/dt(\pi^- p \to \rho^0 n)$ at 4.42 (Ref. 30), 6.0 (solid dots, Ref. 33; crosses, Ref. 31), 7.0 (Ref. 34), and 17.2 GeV/c (Ref. 35). The normalization of the 17.2-GeV/c data shown in this figure should not be trusted (see Ref. 36).

to fit the flat large-$|t|$ behavior of $\rho_{00}^H d\sigma/dt$ without also producing a dip. The dip for model 1 is not very deep owing to the fact that the real and imaginary parts of $H_{0-;+}^{n=1}$ vanish at different values of $|t|$ (see Fig. 6).

Since in the absence of A_1 exchange $\rho_{00}^H d\sigma/dt$ is given by the square of an $n=1$ amplitude and since angular momentum requires this amplitude to vanish in the forward direction, $\rho_{00}^H d\sigma/dt$ is predicted to vanish in the forward direction. The data clearly show a dipping of $\rho_{00}^H d\sigma/dt$ in the forward direction (Fig. 12), in agreement with this prediction.[16]

5. *Alternative explanation of the behavior of $\rho_{00}^H d\sigma/dt(\pi^- p \to \rho^0 n)$ (model 3): Tests for A_1 exchange*

There is much phenomenological evidence that $n=1$ (flip) amplitudes can be described by pure Regge poles whereas $n=0$ (nonflip) amplitudes must be greatly absorbed.[4] This evidence comes from pseudoscalar production where only natural-parity exchanges are allowed (no π exchange). Suppose one wants to generalize and hypothesize that also for vector-meson production only $n=0$ amplitudes should be absorbed and $n=1$ and 2 amplitudes should be described by pure Regge poles. Can one fit the vector-meson production with such a scheme, and, in particular, how does one explain the dip or change in slope of $\rho_{00}^H d\sigma/dt$ $(\pi^- p \to \rho^0 n)$?

One can fit the data on $\pi^- p \to \rho^0 n$ including the change in slope of $\rho_{00}^H d\sigma/dt$ with only $n=0$ (nonflip) absorption if one is willing to include A_1 exchange. Model 3 consists of π, A_1, and A_2 Regge exchanges with only $n=0$ absorption. This $n=0$ absorption is calculated using the same method and parameters as model 2 (square-cut absorption, curve 2, Fig. 3). The quantity $\rho_{00}^H d\sigma/dt(\pi^- p \to \rho^0 n)$ now receives contributions from the amplitude $H_{0-;+}^{n=1}$ (π exchange) *and* the helicity-nonflip amplitude $H_{0+;+}^{n=0}$ (A_1 plus A_1 cut). The change in slope of $\rho_{00}^H d\sigma/dt$ is due to the emergence of the A_1 cut arising from the large $n=0$ absorption. This is shown in Fig. 13. It should be noted that this mechanism produces a change in slope without also producing a dip.

The question now arises as to how a model with A_1 exchange (like model 3) can be distinguished experimentally from models with no A_1 exchange (like models 1 and 2).[17] It is an easy matter to show that the polarized-target asymmetry A is made of three terms

$$A = A_N^1 + A_u^1 + A_u^0, \tag{2.5}$$

and that the recoil-nucleon polarization is given by

$$P_r = A_N^1 - A_u^1 - A_u^0, \tag{2.6}$$

where

$$A_N^1 \frac{d\sigma}{dt} = K \operatorname{Im}(H_{\mathrm{nf}}^N H_{\mathrm{f}}^{N*}), \tag{2.7a}$$

$$A_u^1 \frac{d\sigma}{dt} = -K \operatorname{Im}(H_{\mathrm{nf}}^U H_{\mathrm{f}}^{U*}), \tag{2.7b}$$

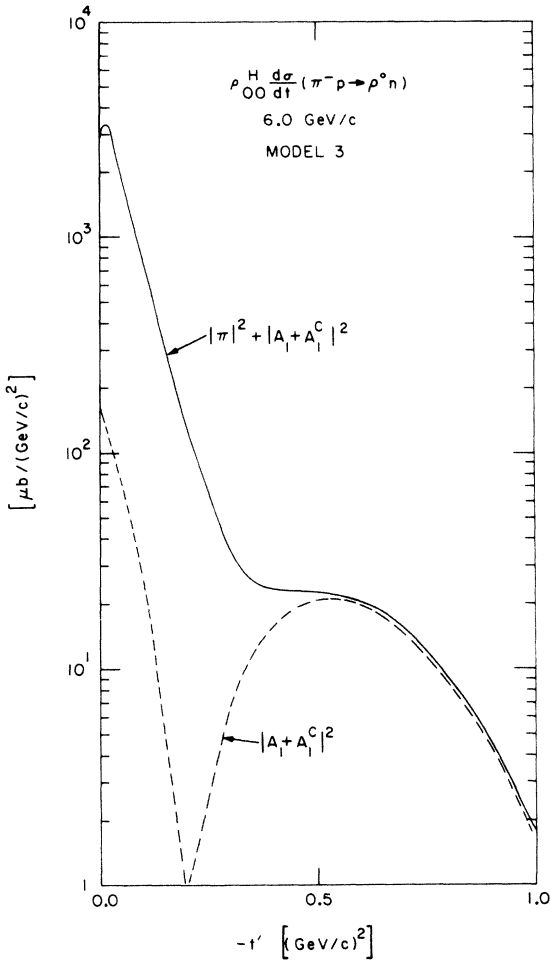

FIG. 13. Contributions to $\rho_{00}^{H}d\sigma/dt\,(\pi^-p\to\rho^0n)$ at 6.0 GeV/c from model 3 (square-cut absorption; only $n=0$ absorption; includes A_1 contribution). In this model the change in slope of this observable is due to the A_1 cut.

$$A_u^0\frac{d\sigma}{dt}=-2K\,\mathrm{Im}(H_{0+;+}H^*_{0-;+}), \tag{2.7c}$$

where

$$H_f^N(s,t)=H^{n=2}_{1-;+}(s,t)+H^{n=0}_{-1-;+}(s,t), \tag{2.8a}$$

$$H_{nf}^N(s,t)=H^{n=1}_{1+;+}(s,t)+H^{n=1}_{-1+;+}(s,t), \tag{2.8b}$$

$$H_f^U(s,t)=H^{n=2}_{1-;+}(s,t)-H^{n=0}_{-1-;+}(s,t), \tag{2.8c}$$

$$H_{nf}^U(s,t)=H^{n=1}_{1+;+}(s,t)-H^{n=1}_{-1+;+}(s,t). \tag{2.8d}$$

To order $1/s$ $A_N^1 d\sigma/dt$ measures the interference between amplitudes with natural parity in the t channel and A_u^1 (A_u^0) measures the interference between amplitudes with unnatural-parity coupling to vector-meson helicity ±1 (0) states. For the reaction $\pi^-p\to\rho^0n$ H_{nf}^U and $H_{0+;+}$ couple to order $1/s$ to A_1 exchange. Thus A_u^1 and A_u^0 measure interferences between π and A_1 exchanges.[17] In the absence of A_1 exchange $A_u^1=A_u^0=0$ and $P_r=A$ (to order $1/s$). Figure 14 shows the quantities A_N^1, A_u^1, A_u^0, A, and P_r predicted for $\pi^-p\to\rho^0n$ from model 3. It can be seen that A_u^1 and A_u^0 are not zero and $A\neq P_r$. In fact, since A_N^1 is small, model 3 has $A\approx -P_r$. Models 1 and 2 have $A_N^1\approx 0$. This is because we set $\gamma_{++}^{A_2}=0$, resulting in $H_{nf}^N=0$. This is undoubtedly an approximation, and we do not expect A_N^1 to be zero experimentally.[17] In any case experimental measurement of A_u^1 and A_u^0 for ρ^0 production will answer the question as to the amount of A_1 exchange present.

6. *Behavior of $\rho_+^H(\pi^-p\to\rho^0n)$: A_2 pole versus π cut*

The large $n=0$ absorption necessary to predict correctly the observed forward spike in $\rho_{11}^H d\sigma/dt$ results in ρ_+^H receiving a large contribution from the π cut. Figure 15 shows ρ_+^H before and after absorption is applied. Before absorption ρ_+^H is given entirely by the A_2 pole, whereas with absorption present it receives an additional contribution from the π cut (and A_2 cut). The quantity $\rho_+^H d\sigma/dt$ is given by the sum of the squares of the amplitudes H_f^N and H_{nf}^N. These amplitudes project out (to order $1/s$) natural parity in the t channel (with no absorption they project out A_2 exchange). Figure 7 shows how in the presence of absorption H_f^N receives a large π-cut contribution. The $n=2$ amplitude $H^{n=2}_{1-;+}$ has a small π cut, while the $n=0$ amplitude $H^{n=0}_{-1-;+}$ has a large one. Thus, when forming the sum the π cut does not cancel out as does the π pole. Another way of saying

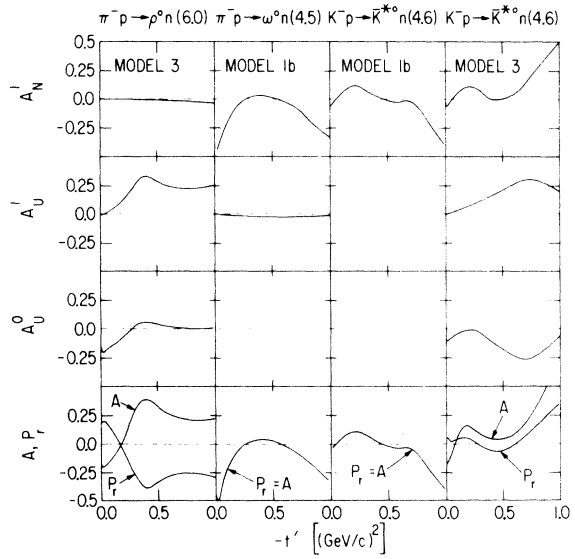

FIG. 14. Predicted polarized target observables A_N^1, A_u^1, A_u^0 [$A=A_N^1+A_u^1+A_u^0$; see (2.5)] and the recoil-nucleon polarization P_r [$P_r=A_N^1-A_u^1-A_u^0$; see (2.6)] from model 3 (includes A_1 contribution) and model 1b (no A_1 contribution).

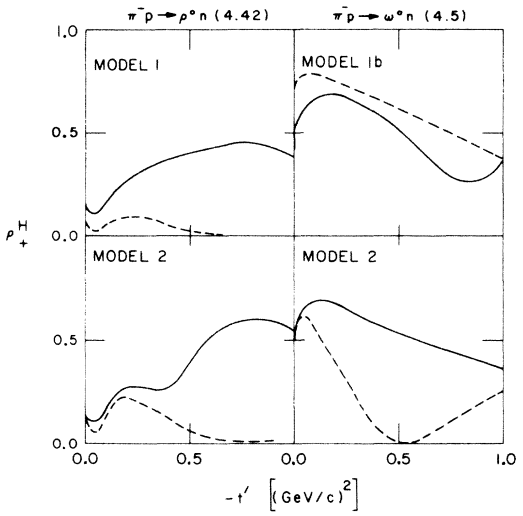

FIG. 15. The observable ρ_+^H ($\rho_+^H = \rho_{11}^H + \rho_{1-1}^H$) for ρ^0 production at 4.42 GeV/c and ω^0 production at 4.5 GeV/c for model 1 (fancy Pomeron absorption), model 1b (fancy Pomeron absorption, no WSNZ for ρ trajectory), model 2 (square-cut absorption; includes WSNZ for ρ trajectory). The solid (dashed) curves are the values after (before) absorption corrections are applied.

this is that the π cut has a large natural-parity component that contributes to H_1^N and hence to ρ_+^H.

7. Energy dependences: Possible trouble spot

Figure 4 shows that the two models give the correct energy dependence for the total ρ^0 production differential cross section. However, both models predict shrinkage of the observable $\rho_{00}^H d\sigma/dt$, and the 17.2-GeV/c data in Fig. 12 show little or no shrinkage. We originally chose a pion trajectory slope of $\alpha_\pi' = 1.0$ GeV^{-2}, but the predicted shrinkage was in such disagreement with the 17.2-GeV/c data that we reduced it to 0.5 GeV^{-2}. We feel that further reduction of the pion-pole slope spoils the notion that the pion is a Regge trajectory (it approaches a fixed pole). This observed lack of shrinkage of $\rho_{00}^H d\sigma/dt$ is seen more clearly in Fig. 16, where we compare the recent data on ρ^0 production at 6.0 GeV/c with the 17.2-GeV/c data. We normalized the data shown in this figure by requiring $\rho_{00}^H d\sigma/dt$ to agree at 6.0 and 17.2 GeV/c in the forward direction. One can see that the 6.0- and 17.2-GeV/c data for $\rho_{00}^H d\sigma/dt$ nearly lie on top of one another. There is very little if any shrinkage. This is quite disturbing since any model where the π is considered a Regge pole (with $\alpha_\pi' > 0$) will predict shrinkage similar to that seen in Fig. 12.

Also shown in Fig. 16 is a large relative increase of $\rho_+^H d\sigma/dt(\pi^- p \to \rho^0 n)$ in going from 6.0 to

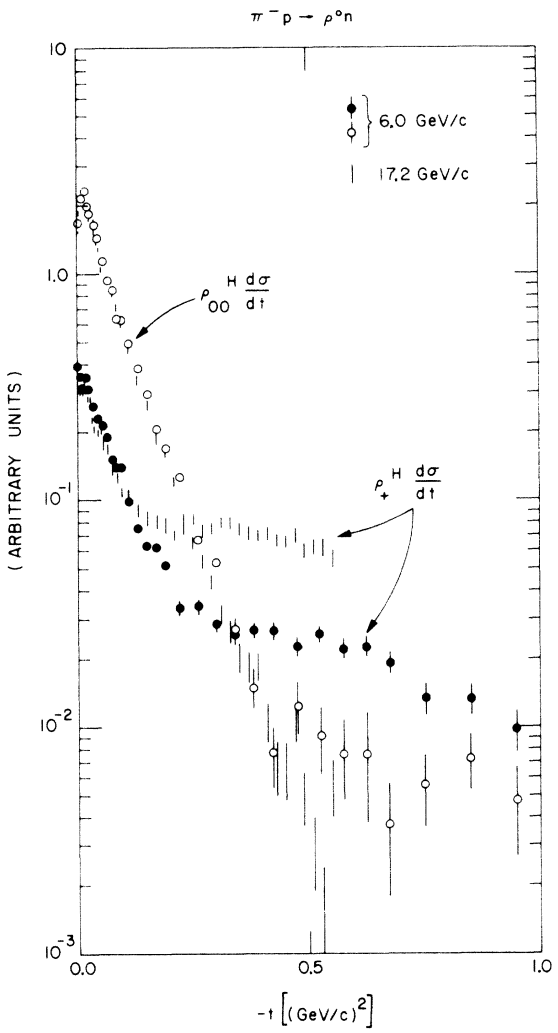

FIG. 16. Comparison of the 6.0-(Ref. 33) and 17.2-GeV/c (Ref. 35) $\pi^- p \to \rho^0 n$ data. The data are normalized so that $\rho_{00}^H d\sigma/dt$ is the same in the forward direction at the two energies. The figure shows the lack of shrinkage of $\rho_{00}^H d\sigma/dt$ and the relative increase of the natural-parity projection $\rho_+^H d\sigma/dt$ ($\rho_+^H = \rho_{11}^H + \rho_{1-1}^H$).

17.2 GeV/c. One can determine from this figure that for $0.3 \lesssim |t| \lesssim 0.6$ GeV/c $\Delta\alpha_{\text{eff}} \approx 0.4$–$0.5$, where $\Delta\alpha_{\text{eff}}$ is the difference between the effective α for $\rho_+^H d\sigma/dt$ and $\rho_{00}^H d\sigma/dt$ (remember α_{eff} for $\rho_{00}^H d\sigma/dt$ is almost flat and ≈ 0). This large relative increase of $\rho_+^H d\sigma/dt$ is *not* predicted by model 1 or model 2 [model 1 (2) has an α_{eff} for $\rho_+^H d\sigma/dt$ of ≈ -0.5 (≈ -0.2) at $t = -0.6$ (GeV/c)^2]. Figure 17 shows the α_{eff} for the π-cut contributions to $\rho_+^H d\sigma/dt$, which is seen to lie much lower than the α_{eff} resulting from the A_2 pole. The models have large absorption and therefore most of $\rho_+^H(\pi^- p \to \rho^0 n)$ is due to the π cut (see Fig. 15), which results in an energy dependence of $\rho_+^H d\sigma/dt$

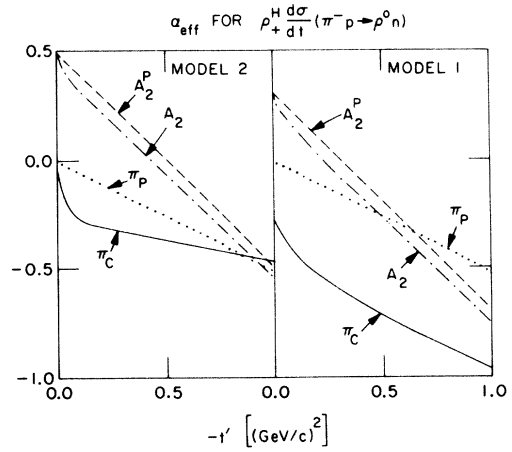

FIG. 17. Shows the effective α's (α_{eff}) between 4.0 and 16.0 GeV/c of the various contributions to $\rho_+^H d\sigma/dt$ ($\pi^- p \to \rho^0 n$) from model 1 (fancy Pomeron absorption) and model 2 (square-cut absorption). For comparison we also show the α_{eff} of the input π pole (π_P) and the input A_2 pole (A_2^P). The A_2 contribution to $\rho_+^H d\sigma/dt$ lies slightly lower than the input A_2 pole because of nonasymptotic angular factors. The two models differ markedly in the energy dependence of the π cut (π_C).

which is closer to that of the π cut rather than the A_2 pole.

Figure 9 shows that model 1 is better able to fit the energy dependence of the small-$|t|$ behavior of $\rho_{11}^H d\sigma/dt(\pi^- p \to \rho^0 n)$. This is because the small-$|t|$ values of $\rho_{11}^H d\sigma/dt$ are given primarily by the π cut, and model 1 has a π cut which decreases faster with energy than model 2 (see Fig. 17).

B. Reactions $\pi^- p \to \omega^0 n$ and $\pi^+ n \to \omega^0 p$

1. *Models 1a, 1b, and 2: Fitting procedure*

We adopt the philosophy that the absorption for the reactions $\pi N \to \omega^0 N$ is the same as that required for the reactions $\pi N \to \rho^0 N$. We apply models to ω^0 production that have the same amount of absorption that we found necessary in fitting ρ^0 production.

We found that for ρ^0 production it was necessary to have the real parts of the ρ and A_2 Regge exchanges contribute with the same sign to the amplitude $H_{-1-;+}^{n=0}$ (see Sec. II A 2). This fixed the phase between the π and A_2 Regge exchanges. For ω^0 production we must decide whether the ρ and B Regge exchanges contribute in phase or out of phase to the amplitude $H_{-1-;+}^{n=0}$. The two possibilities are illustrated in Fig. 19. Case 1 has the ρ and B pole contributing destructively, which results in a relative ω^0/ρ^0 production phase $\beta_N^{\text{pole}} = 90°$. In case 1 the ρ and A_2 Regge poles have the relative phase predicted from EXD arguments for the reaction $K^- p \to \bar{K}^{*0} n$ (see Table I). Case 2 has the ρ and B poles contribution in phase to $H_{-1-;+}^{n=0}$, which results in $\beta_N^{\text{pole}} = -90°$. Here the ρ and A_2 have relative phase in $K^- p \to \bar{K}^{*0} n$ opposite to that predicted by EXD arguments. Since model 1 abandons the notion of EXD for the Regge poles, we divide model 1 into two cases for the reactions $\pi N \to \omega^0 N$. Model 1a has case-2-type phases and model 1b has case-1-type phases.

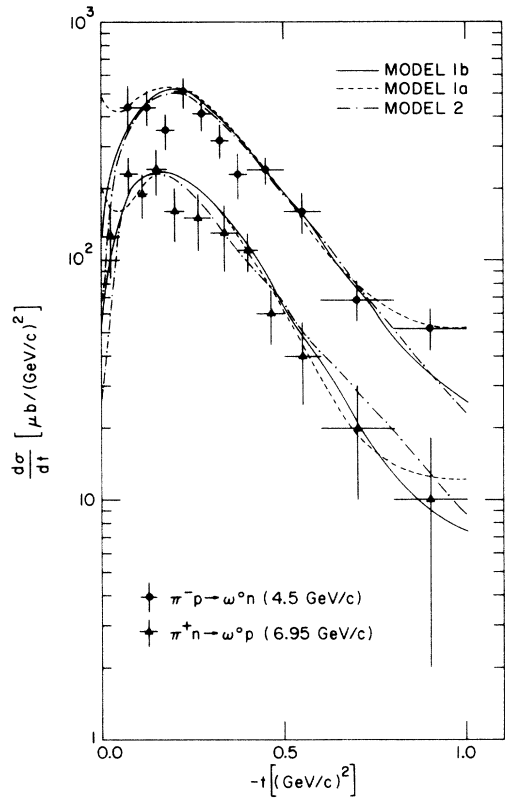

FIG. 18. Comparison of model 1a (fancy Pomeron absorption; uses opposite of EXD ρ-A_2 phase prediction), model 1b (fancy Pomeron absorption; uses EXD-predicted ρ-A_2 phase), and model 2 (square-cut absorption; uses EXD-predicted ρ-A_2 phase) with the differential cross section for $\pi^- p \to \omega^0 n$ at 4.5 GeV/c (Ref. 37) and $\pi^+ n \to \omega^0 p$ at 6.95 GeV/c (Ref. 38). Models 1a and 1b do not use a WSNZ for the ρ trajectory, whereas model 2 does.

(a) Model 1a. This model is identical to model 1 of Sec. III A 1 and has the relative ρ-B phase of case 2 in Fig. 19 (opposite to the EXD predicted phase). We fit the differential cross section and vector-meson density-matrix elements at 4.5 GeV/c using ρ and B exchange with trajectories $\alpha_\rho(t) = 0.5 + 1.0t$ and $\alpha_B(t) = \alpha_\pi(t) = 0.5(t - m_\pi^2)$. We fit only the 4.5-GeV/c $\pi^- p \to \omega^0 n$ data. The observables for $\pi N \to \omega^0 N$ at other energies are predicted. In Fig. 18 we compare the model with the differential cross sections for $\pi^- p \to \omega^0 n$ at 4.5 GeV/c

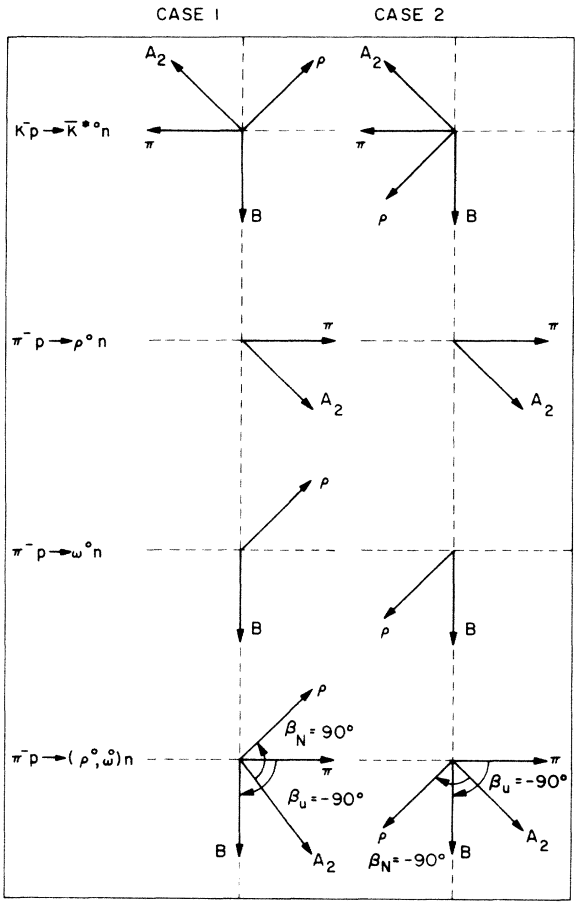

FIG. 19. Argand diagram of the Regge-pole phases at $t = 0.0$ (GeV/c)^2 for the amplitude $H^{n=0}_{-1\,;+}$ and the reactions $K^-p \to \bar{K}^{*0}n$, $\pi^-p \to \rho^0 n$, and $\pi^-p \to \omega^0 n$. In case 1 the ρ and A_2 have the relative phase predicted by EXD arguments, whereas in case 2 the ρ and A_2 have the opposite phase. In both cases the π-B relative phase is as predicted by EXD and the predicted unnatural-parity relative ω^0/ρ^0 phase is $\beta_u = 90°$. The relative ω^0/ρ^0 phase for the natural parity ρ and A_2 poles in $\beta_N = 90°$ for case 1 and $\beta_N = -90°$ for case 2.

TABLE I. SU(3) factors used to relate the six charge-exchange vector-meson production reactions under study. Entries in the table are $d\gamma^R$, where d is the SU(3) factor and $\gamma^R = \gamma_{\lambda_3 \lambda_4;\lambda_2}(t)$ is the residue of the Regge pole R.

Reaction \ R	π	B	ρ	A_2	A_1
$K^-p \to \bar{K}^{*0}n$	γ^π	γ^B	γ^ρ	γ^{A_2}	γ^{A_1}
$K^+n \to K^{*0}p$	γ^π	$-\gamma^B$	$-\gamma^\rho$	γ^{A_2}	γ^{A_1}
$\pi^-p \to \rho^0 n$	$-\sqrt{2}\,\gamma^\pi$	0	0	$-\sqrt{2}\,\gamma^{A_2}$	$-\sqrt{2}\,\gamma^{A_1}$
$\pi^+n \to \rho^0 p$	$-\sqrt{2}\,\gamma^\pi$	0	0	$-\sqrt{2}\,\gamma^{A_2}$	$-\sqrt{2}\,\gamma^{A_1}$
$\pi^-p \to \omega^0 n$	0	$\sqrt{2}\,\gamma^B$	$\sqrt{2}\,\gamma^\rho$	0	0
$\pi^+n \to \omega^0 p$	0	$-\sqrt{2}\,\gamma^B$	$-\sqrt{2}\,\gamma^\rho$	0	0

and for $\pi^+n \to \omega^0 p$ at 6.95 GeV/c. In Fig. 20 we compare the model with the vector-meson density-matrix elements for $\pi^-p \to \omega^0 n$ at 4.5 and 5.5 GeV/c, and in Fig. 21 for $\pi^+n \to \omega^0 p$ at 6.0 and 6.95 GeV/c. The Regge-pole and cut contributions to the s-channel helicity amplitudes for $\pi^-p \to \omega^0 n$ at 4.0 GeV/c at $t_0 - t = -0.1$ GeV/c are shown in the Argand diagrams of Fig. 22.

(b) Model 1b. This model is identical to model 1 of Sec. II A 1 and has the relative ρ-B phase of case 1 in Fig. 19 (EXD predicted phase). The trajectory functions are the same as model 1a. Figure 18 shows a comparison of this model with the differential cross sections for $\pi^-p \to \omega^0 n$ at 4.5 GeV/c and $\pi^+n \to \omega^0 p$ at 6.75 GeV/c. In Fig. 20 the model is compared with the vector-meson density-matrix elements for $\pi^-p \to \omega^0 n$ at 4.5 and 5.5 GeV/c and in Fig. 21 with the density-matrix elements for $\pi^+n \to \omega^0 p$ at 6.0 and 6.95 GeV/c. The Regge-pole and cut contributions to the s-channel helicity amplitudes for $\pi^-p \to \omega^0 n$ at 4.0 GeV/c and with $t - t_0 = -0.1$ GeV/c are shown in the Argand diagrams of Fig. 22. In Fig. 23 we show various contributions to the $\pi^-p \to \omega^0 n$ differential cross sec-

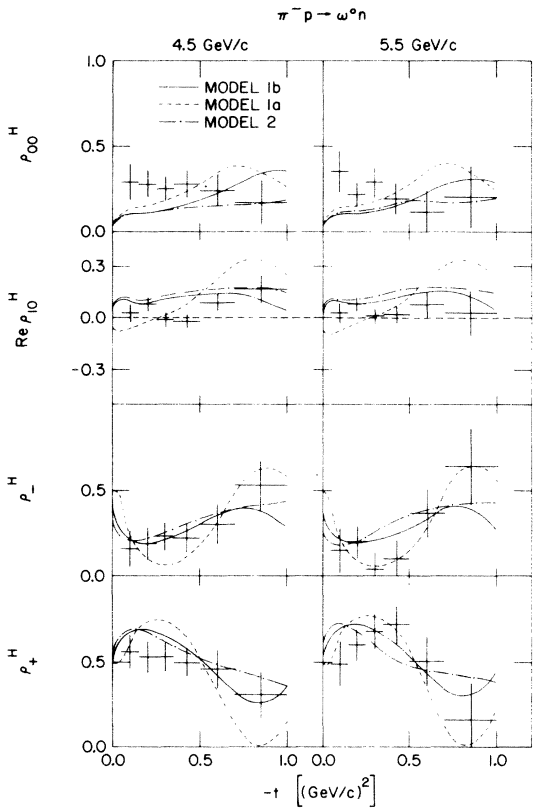

FIG. 20. Comparison of the three models in Fig. 18 with the data on the vector-meson density-matrix elements ($\rho^H_\pm = \rho^H_{11} \pm \rho^H_{1-1}$) for the reaction $\pi^-p \to \omega^0 n$ at 4.5 and 5.5 GeV/c (Ref. 37).

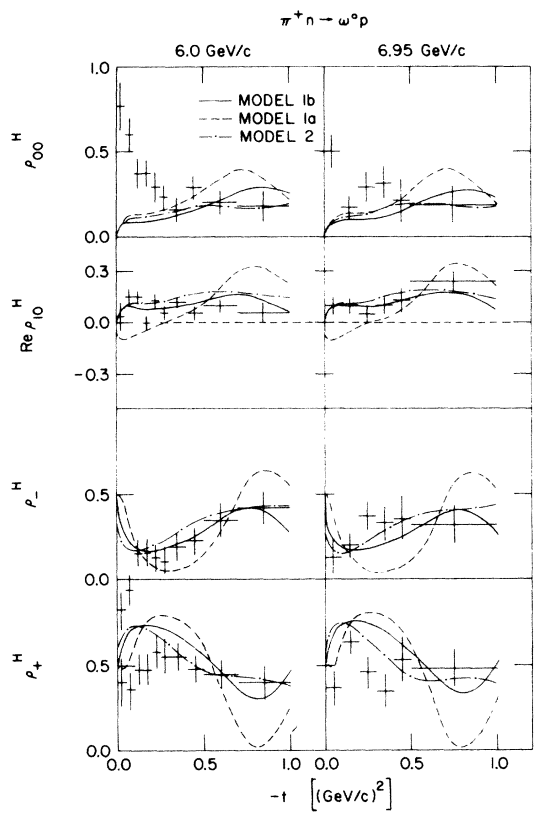

FIG. 21. Comparison of the three models in Fig. 18 with the data on the vector-meson density-matrix elements ($\rho^H_\pm = \rho^H_{11} \pm \rho^H_{1-1}$), for the reaction $\pi^+ n \to \omega^0 p$ at 6.0 (Ref. 39) and 6.95 GeV/c (Ref. 38). The first two bins of the 6.0-GeV/c data should not be trusted (see Ref. 40).

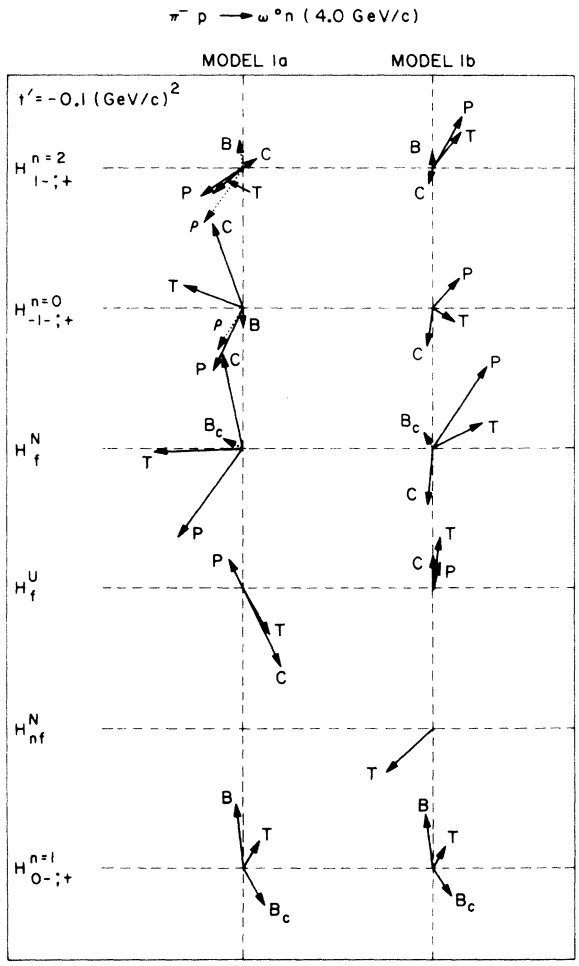

FIG. 22. Argand diagram of the various contributions to the s-channel helicity amplitudes at 4.0 GeV/c and $t' \equiv t - t_0 = -0.1$ (GeV/c)^2 for model 1a (fancy Pomeron absorption; uses opposite of EXD ρ-A_2 relative phase prediction) and model 1b (fancy Pomeron absorption; uses EXD ρ-A_2 relative phase prediction). The labels P and C correspond to the total pole ($\rho + B$) and total cut ($\rho_C + B_C$) contributions, respectively. The resulting total amplitude (pole + cut) is labeled T.

tion at 4.5 GeV/c resulting from model 1b.

(c) Model 2. This model is identical to model 2 of Sec. II A 1 and has the relative ρ-B phase of case 1 in Fig. 19 (EXD predicted phase). We again fit the 4.5-GeV/c $\pi^- p \to \omega^0 n$ data using a ρ and B Regge pole with trajectories $\alpha_\rho(t) = \alpha_{A_2}(t) = 0.5 + 1.0t$ and $\alpha_B(t) = \alpha_\pi(t) = 0.5(t - m_\pi{}^2)$. This model includes a WSNZ for the ρ trajectory. In Fig. 18 we compare the model with the differential cross sections for $\pi^- p \to \omega^0 n$ at 4.5 GeV/c and $\pi^+ n \to \omega^0 p$ at 6.95 GeV/c. In Fig. 20 the model is confronted with the vector-meson density-matrix elements for $\pi^- p \to \omega^0 n$ at 4.5 and 5.5 GeV/c and in Fig. 21 with those for $\pi^+ n \to \omega^0 p$ at 6.0 and 6.95 GeV/c.

2. Behavior of $\rho^H_+(\pi N \to \omega^0 N)$: ρ pole versus B cut

Just as $\rho^H_+(\pi^- N \to \rho^0 N)$ receives a contribution from the π cut (see Sec. II A 6), so does $\rho^H_+(\pi N \to \omega^0 N)$ receive a contribution from the B cut. The mechanism by which the ω^0 production amplitude H^N_f receives B-cut contributions (see Fig. 22) is identical to the mechanism (explained in Sec. II A 6) by which the ρ^0 production amplitude H^N_f receives π-cut contributions (Fig. 7). It has been argued that since $\rho^H_+(\pi^- p \to \omega^0 n)$ projects out the ρ-exchange contribution, the lack of a dip at $t = -0.6$ (GeV/c)^2 in this observable (Figs. 20 and 21) implies that the ρ pole does not have a WSNZ. This is obviously fallacious since both model 1 (no WSNZ for ρ) and model 2 (with WSNZ for ρ) are able to fit $\rho^H_+(\pi N \to \omega N)$. The point is that even if the ρ-pole contribution to ρ^H_+ vanishes at $t = -0.6$ (GeV/c)^2 the B-cut contribution will fill in this dip. This is shown in Fig. 15, where the contributions to ρ^H_+ are shown before and after absorption (also see Fig. 23).

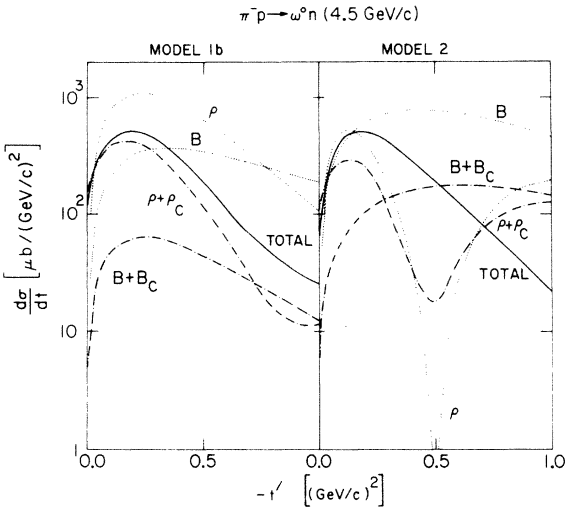

FIG. 23. Contributions to the differential cross section for $\pi^- p \to \omega^0 n$ at 4.5 GeV/c from model 1b (fancy Pomeron absorption; no WSNZ for ρ) and model 2 (square-cut absorption; uses WSNZ for ρ).

3. *Behavior of* $\rho_{00}^H d\sigma/dt(\pi N \to \omega^0 N)$: *Where do helicity-zero* ω^0*'s come from?*[18]

The observable $\rho_{00}^H d\sigma/dt(\pi N \to \omega^0 N)$ is proportional to the square of the $n=1$ amplitude $H^{n=1}_{0-;+}$, which receives contributions from B exchange. This amplitude vanishes in the forward direction by angular momentum conservation, and thus one expects very few small-$|t|$ ω^0's to be produced in $\pi N \to \omega^0 N$. Figure 24 shows that the data on $\rho_{00}^H d\sigma/dt(\pi N \to \omega^0 N)$ are consistently larger for small $|t|$ than the model predictions, particularly for the reaction $\pi^+ n \to \omega^0 p$. Where do these extra helicity-zero ω^0's come from?

It is obvious that ρ-ω mixing allows π exchange to contribute to $\rho_{00}^H d\sigma/dt(\pi N \to \omega^0 N)$ [see Fig. 25(a)]. Given the amplitudes for ρ^0 and ω^0 production from our model fits, we predict the s-channel helicity

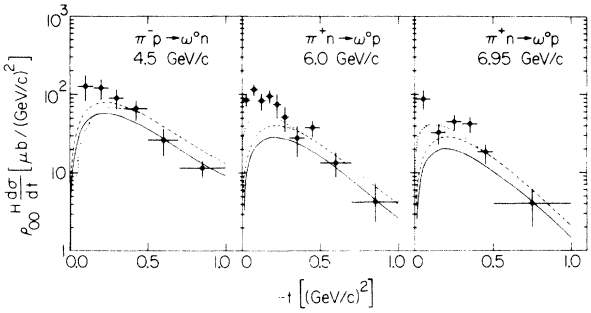

FIG. 24. Comparison of model 1b (solid curves) and model 1a (dashed curves) with the data on $\rho_{00}^H d\sigma/dt$ for $\pi^- p \to \omega^0 n$ at 4.5 GeV/c (Ref. 37) and for $\pi^+ n \to \omega^0 p$ at 6.0 (Ref. 39) and 6.95 GeV/c (Ref. 38). The dotted curve shows the effect on model 1a of including ρ-ω mixing with $\delta = 4.0$ MeV.

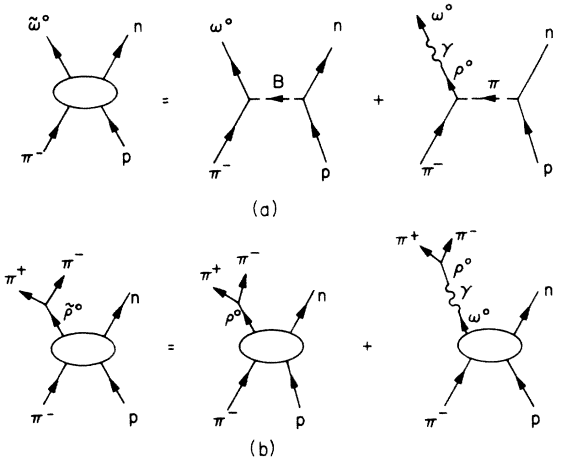

FIG. 25. Illustration of two ρ-ω mixing effects: (a) shows how ρ-ω mixing allows π exchange to contribute to the reaction $\pi^- p \to \tilde{\omega}^0 n$; (b) shows how ρ-ω mixing affects the $\pi^+\pi^-$ mass spectra for the reaction $\pi^- p \to \pi^+\pi^- n$.

amplitudes for production of the electromagnetically mixed $\tilde{\rho}^0$ and $\tilde{\omega}^0$ mesons using

$$H^{\pi N \to \tilde{\rho}^0 N}_{\lambda_3\lambda_4;\lambda_1\lambda_2}(s,t) = H^{\pi N \to \rho^0 N}_{\lambda_3\lambda_4;\lambda_1\lambda_2}(s,t) - \epsilon H^{\pi N \to \omega^0 N}_{\lambda_3\lambda_4;\lambda_1\lambda_2}(s,t), \tag{2.9a}$$

$$H^{\pi N \to \tilde{\omega}^0 N}_{\lambda_3\lambda_4;\lambda_1\lambda_2}(s,t) = \epsilon H^{\pi N \to \rho^0 N}_{\lambda_3\lambda_4;\lambda_1\lambda_2}(s,t) + H^{\pi N \to \omega^0 N}_{\lambda_3\lambda_4;\lambda_1\lambda_2}(s,t), \tag{2.9b}$$

where ϵ is a reasonably well-known quantity determined from $e^+e^- \to \pi^+\pi^-$ experiments.[19-22]

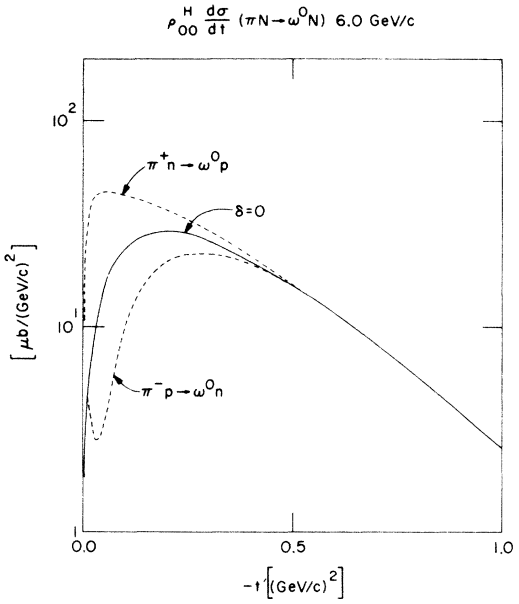

FIG. 26. The predicted amount of isospin violation in the observable $\rho_{00}^H d\sigma/dt\,(\pi N \to \omega^0 N)$ at 6.0 GeV/c using model 1b with ρ-ω mixing parameter $\delta = 4.0$ MeV.

Figure 24 shows the effect of ρ-ω mixing on $\rho_{00}^H d\sigma/dt(\pi N \to \omega^0 N)$ using a value of the ρ-ω mixing parameter $\delta = 4.0$ MeV. We see that the reaction $\pi^+ n \to \tilde{\omega}^0 p$ has substantially more helicity-zero ω^0's than the unmixed reaction $\pi^+ n \to \omega^0 p$ [a factor of about 3–4 at $p_{\text{lab}} = 6.0$ GeV/c and $t = -0.05$ (GeV/c)^2], whereas the reaction $\pi^- p \to \tilde{\omega}^0 n$ has less helicity-zero ω^0's than the unmixed case. It remains for future experiments with higher statistics to verify these predictions.

4. *Isospin violations due to ρ-ω mixing*

In the absence of ρ-ω mixing isospin conservation predicts the amplitudes and hence the observables for $\pi^- p \to \omega^0 n$ to be identical to those for $\pi^+ n \to \omega^0 p$ at a given energy. It is well known that ρ-ω mixing will cause violations of this prediction.[23] The effect is greatest in the observable $\rho_{00}^H d\sigma/dt(\pi N \to \omega^0 N)$, which owing to the ρ-ω mixing can receive a contribution from π exchange [Fig. 25(a)]. In Fig. 26 we use the amplitudes from model 1b with $\delta = 4.0$ MeV to predict the isospin violations of the observable $\rho_{00}^H d\sigma/dt(\pi N \to \tilde{\omega}^0 N)$ at 6.0 GeV/c. At $t = -0.05$ (GeV/c)^2 the two reactions $\pi^- p \to \omega^0 n$ and $\pi^+ n \to \omega^0 p$ are seen to differ by about a factor of 10. The effect depends on the size of the electromagnetic mixing parameter δ, and a value of 4.0 MeV is probably an upper limit (theory predicts 2.5 MeV).[19-22] Thus the curves in Fig. 26 probably illustrate the upper limit of this effect.

5. *Unmeasured observables*

Figure 14 shows the predicted values for the as-yet-unmeasured polarized-target asymmetry and recoil-nucleon polarization observables resulting from model 1b for $\pi^- p \to \omega^0 n$ at 4.5 GeV/c. Since we have not included the EXD partner of the A_1 ($\tau = -1$, $C = -1$, $\eta = -1$) the observables A_u^1 and A_u^0 are zero (to order $1/s$) and $P_r = A$. The nonzero values of P_r (and A) are produced by the ρ and ρ-cut which contribute to A_N^1.

C. π-π mass spectra: ρ-ω interference

Given the model determinations of the s-channel helicity amplitudes for ρ^0 production (Sec. II A) and ω^0 production (Sec. II B) the $\pi^+\pi^-$ mass spectra for $\pi N \to (\pi^+\pi^-)N$ can now be predicted (including ρ-ω mixing). The s-channel helicity amplitudes resulting from these models are used to calculate the ρ^0/ω^0 amplitude ratios

$$R^{\pi N}_{\lambda_3\lambda_4;\lambda_2}(s,t) = H^{\pi N\to\omega^0 N}_{\lambda_3\lambda_4;\lambda_2}(s,t)/H^{\pi N\to\rho^0 N}_{\lambda_3\lambda_4;\lambda_2}(s,t) = |R^{\pi N}_{\lambda_3\lambda_4;\lambda_2}(s,t)|\exp[\,i\beta^{\pi N}_{\lambda_3\lambda_4;\lambda_2}(s,t)] \tag{2.10}$$

from which the $\pi^+\pi^-$ production amplitudes can be determined as follows[22]:

$$S^{\pi N\to(\pi^+\pi^-)N}_{\lambda_3\lambda_4;\lambda_2}(s,t,m) = H^{\pi N\to\rho^0 N}_{\lambda_3\lambda_4;\lambda_2}(s,t)T(\rho\to\pi^+\pi^-) \times \frac{[1+\delta R^{\pi N}_{\lambda_3\lambda_4;\lambda_2}(s,t)/(m_\omega - m - \frac{1}{2}i\Gamma_\omega)]}{m_\rho - m - \frac{1}{2}i\Gamma_\rho}. \tag{2.11}$$

There is a modification of the $\pi^+\pi^-$ mass spectrum due to the quantity in the square brackets in (2.11). At the ω^0 mass this quantity becomes

$$1 + 2i(\delta/\Gamma_\omega)|R^{\pi N}_{\lambda_3\lambda_4;\lambda_2}(s,t)|\exp[\,i\beta^{\pi N}_{\lambda_3\lambda_4;\lambda_2}(s,t)], \tag{2.12}$$

which causes a spike (dip) for $\beta = -\frac{1}{2}\pi$ ($\frac{1}{2}\pi$). Also, since $R^{\pi^- p}_{\lambda_3\lambda_4;\lambda_2}$ and $R^{\pi^+ N}_{\lambda_3\lambda_4;\lambda_2}$ have opposite signs, a spike (dip) in $\pi^- p \to (\pi^+\pi^-)n$ becomes a dip (spike) in $\pi^+ n \to (\pi^+\pi^-)p$. In general the ratio $R^{\pi N}_{\lambda_3\lambda_4;\lambda_2}(s,t)$ can be different for each helicity amplitude.

Following Goldhaber, Fox, and Quigg[22] the relative production phase $\beta^{\pi N}_{\lambda_3\lambda_4;\lambda_2}(s,t)$ can be estimated from SU(3) and EXD. Using SU(3) (Table I) one arrives at

$$\frac{H^{\pi^- p\to\omega^0 n}_{(B\text{ exchange})}}{H^{\pi^- p\to\rho^0 n}_{(\pi\text{ exchange})}} = \frac{(2)^{1/2}\gamma_B(t)\{\,i + \tan[\,\frac{1}{2}\pi\alpha_B(t)]\,\}}{-(2)^{1/2}\gamma_\pi(t)\{\,i - \cot[\,\frac{1}{2}\pi\alpha_\pi(t)]\,\}} = i\,\frac{\gamma_B(t)}{\gamma_\pi(t)}\tan[\,\tfrac{1}{2}\pi\alpha_u(t)], \tag{2.13}$$

where it is assumed that $\alpha_\pi(t) = \alpha_B(t) = \alpha_u(t)$. If one further assumes that the residues γ_B and γ_π have the same sign (strong EXD predicts them to be equal), then since $\alpha_u(t) < 0$

$$\beta^{\pi^- p}(\pi, B\text{ exchange}) = -\tfrac{1}{2}\pi. \tag{2.14}$$

This is illustrated in Fig. 19. Similarly, one has

$$\frac{H^{\pi^- p\to\omega^0 n}_{(\rho\text{ exchange})}}{H^{\pi^- p\to\rho^0 n}_{(A_2\text{ exchange})}} = i\left(\frac{\gamma_\rho(t)}{\gamma_{A_2}(t)}\right)\tan[\,\tfrac{1}{2}\pi\alpha_N(t)], \tag{2.15}$$

where $\alpha_N(t) = \alpha_{A_2}(t) = \alpha_\rho(t)$. Assuming that the residues γ_{A_2} and γ_ρ have the same sign (strong EXD predicts $\gamma_{A_2} = \gamma_\rho$) and noting that $\alpha_N(t) > 0$ for $t < -0.5$ (GeV/c)^2, one arrives at

$$\beta^{\pi^- p}(\rho, A_2\text{ exchange}) = \tfrac{1}{2}\pi. \tag{2.16}$$

We illustrate this in Fig. 19, case 1.

Equation (2.14) predicts that observables that project out unnatural-parity exchange (i.e., $\rho_{00}^H d\sigma/dt\,dm$) have a spike at $m = m_\omega$ for $\pi^- p \to \pi^+\pi^- n$ and a dip for $\pi^+ n \to \pi^+\pi^- p$, while (2.16) predicts that observables that project out natural-parity exchange (i.e., $\rho_+^H d\sigma/dt\,dm$) have a dip at $m = m_\omega$ for $\pi^- p \to \pi^+\pi^- n$ and a spike for $\pi^+ n \to \pi^+\pi^- p$. Until recently data were available only on $d\sigma/dt\,dm$ and showed a spike at $m = m_\omega$ for $\pi^- p \to \pi^+\pi^- n$ and a dip for $\pi^+ n \to \pi^+\pi^- p$ in accordance with the above

estimate since these reactions are predominantly unnatural-parity exchange. Recently, excellent data have become available with good enough statistics to form the projections $\rho^H_{ij}\, d\sigma/dtdm$. Figure 27 shows the quantities $\rho^H_{00} d\sigma/dtdm$, $\rho^H_+ d\sigma/dtdm$, $\rho^H_- d\sigma/dtdm$, and $d\sigma/dtdm$ for the difference between $\pi^- p \to \pi^+\pi^- n$ and $\pi^+ n \to \pi^+\pi^- p$ for $p_{\rm lab} = 4.0$ GeV/c at $0.08 < -t < 0.2$ (GeV/c)^2. The data show peaking at $m = m_\omega$ for *all* projections both natural and unnatural. The peaking of $\rho^H_+ d\sigma/dtdm$ is in disagreement with the naive pole predictions (2.15). There are two ways in which this incorrect prediction can be changed.

(1). It may be true that EXD is broken so badly at small $|t|$ that $(\gamma_\rho/\gamma_{A_2})$ in (2.15) have opposite signs, in which case (2.16) becomes $\beta^{\pi-p}(\rho, A_2$ exchange$) = -\frac{1}{2}\pi$. This is illustrated in Fig. 2, case 2.

(2). The other obvious point is that the prediction (2.16) was made neglecting absorption. The quantity $\rho^H_+ d\sigma/dt$ receives large contributions from the π Regge cut in ρ^0 production and from the B Regge cut in ω^0 production. As we shall see, all Regge absorption models predict the cut to be approximately 180° out of phase with the corresponding pole (destructive cuts).

Thus

$$\beta^{\pi-p}(\pi \text{ cut},\ B \text{ cut}) \approx -\tfrac{1}{2}\pi, \tag{2.17}$$

and if $\rho^H_+ d\sigma/dtdm(\pi^- p \to \pi^-\pi^+ m)$ is predominantly π cut, it will peak at the ω mass even if the natural-parity Regge poles obey (2.16).

In order to avoid normalization problems and to concentrate on ρ-ω interference effects, we calculate the quantity

$$\Delta\rho^H_{ij}\ \frac{d\sigma}{dtdm}(s,t,m) \equiv \frac{\rho^H_{ij}\frac{d\sigma}{dtdm}(\pi^- p) - \rho^H_{ij}\frac{d\sigma}{dtdm}(\pi^+ n)}{\rho^H_{ij}\frac{d\sigma}{dtdm}(\pi^- p) + \rho^H_{ij}\frac{d\sigma}{dtdm}(\pi^+ n)}, \tag{2.18}$$

which we compare with the data at 4.0 GeV/c. Figure 28 shows a comparison of the data with models 1a, 1b, and 2, where we used $\delta = 4.0$ MeV in (2.9). It is seen that all models adequately describe the ρ-ω interference effects for $d\sigma/dtdm$ and $\rho^H_{00} d\sigma/dtdm$, but differ greatly in their ability to describe the ρ-ω interference effects seen in $\rho^H_\pm d\sigma/dtdm$. It is of interest to look in detail into the behavior of the amplitudes that give rise to the predictions shown in Fig. 27 for $\rho^H_\pm d\sigma/dtdm$.

Neglecting, for simplicity, the amplitudes $H^N_{\rm nf}$ and $H^{n=0}_{0+;+}$ we have

$$S^{\pi N\to(\pi^+\pi^-)N}_N(s,t,m) = H^N_{\rm f}(\pi N\to\rho^0 N)T(\rho\to\pi^+\pi^-) \times[1+\delta R^{\pi N}_N(s,t)/d_\omega(m)]/d_\rho(m), \tag{2.19a}$$

$$S^{\pi N\to(\pi^+\pi^-)N}_U(s,t,m) = H^U_{\rm f}(\pi N\to\rho^0 N)T(\rho\to\pi^+\pi^-) \times[1+\delta R^{\pi N}_u(s,t)/d_\omega(m)]/d_\rho(m), \tag{2.19b}$$

$$S^{\pi N\to(\pi^+\pi^-)N}_O(s,t,m) = H^{n=1}_{0-;+}(\pi N\to\rho^0 N)T(\rho\to\pi^+\pi^-) \times[1+\delta R^{\pi N}_0(s,t)/d_\omega(m)]/d_\rho(m), \tag{2.19c}$$

where $d_{\rho,\omega}(m) = m_{\rho,\omega} - m\tfrac{1}{2}i\Gamma_{\rho,\omega}$, and where the amplitude ratios are given by

$$R^{\pi N}_N(s,t) = H^N_{\rm f}(\pi N\to\omega^0 N)/H^N_{\rm f}(\pi N\to\rho^0 N) = |R^{\pi N}_N| e^{i\beta^{\pi N}_N}, \tag{2.20a}$$

$$R^{\pi N}_U(s,t) = H^U_{\rm f}(\pi N\to\omega^0 N)/H^U_{\rm f}(\pi N\to\rho^0 N) = |R^{\pi N}_U| e^{i\beta^{\pi N}_U}, \tag{2.20b}$$

$$R^{\pi N}_0(s,t) = H^{n=1}_{0-;+}(\pi N\to\omega^0 N)/H^{n=1}_{0-;+}(\pi N\to\rho^0 N) = |R^{\pi N}_0| e^{i\beta^{\pi N}_0}. \tag{2.20c}$$

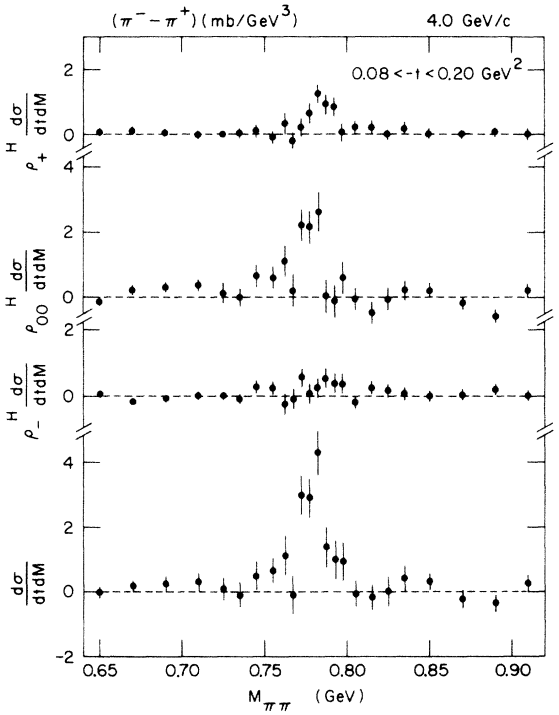

FIG. 27. The ρ-ω interference data from Ref. 29 on the $\pi^+\pi^-$ mass spectra for the reaction $\pi N \to \pi^+\pi^- N$ at 4.0 GeV/c and with $0.08 \le -t \le 0.20$ GeV/c. The observables $\rho^H_{00} d\sigma/dtdm$, $\rho^H_\pm d\sigma/dtdm$, and $d\sigma/dtdm$ for the difference between the reactions $\pi^- p \to \pi^+\pi^- n$ and $\pi^+ n \to \pi^+\pi^- p$ are plotted versus the $\pi^+\pi^-$ mass, where $\rho^H_\pm = \rho^H_{11} \pm \rho^H_{1-1}$.

The amplitudes $H_f^{N,U}$ are defined by (2.8). The observables are then given by

$$\rho_+^H \frac{d\sigma^{\pi N}}{dt\,dm}(s,t,m)=K|S_N^{\pi N}(s,t,m)|^2, \qquad (2.21a)$$

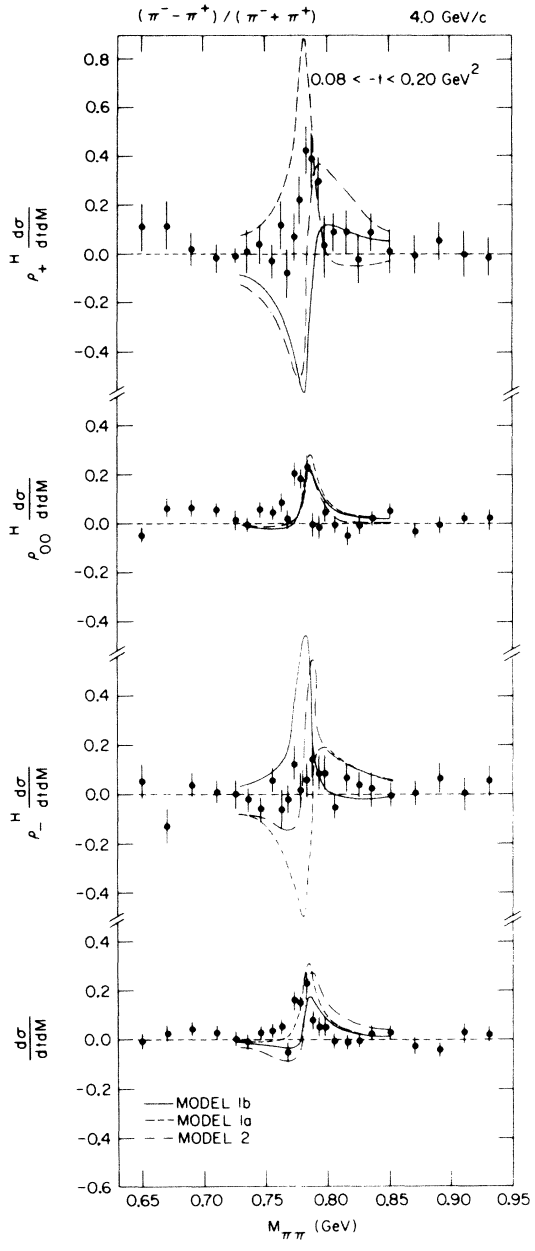

FIG. 28. Comparison of ρ-ω interference effects ($\delta = 4.0$ MeV) predicted from model 1a (fancy Pomeron absorption; uses opposite EXD-predicted ρ-A_2 relative phase), model 1b (fancy Pomeron absorption; uses EXD-predicted ρ-A_2 relative phase), and model 2 (square-cut model; uses EXD-predicted ρ-A_2 relative phase) with the data on $\rho_{00}^H d\sigma/dt\,dm$, $\rho_\pm^H d\sigma/dt\,dm$, and $d\sigma/dt\,dm$ for $\pi N \to \pi\pi N$ at. 4.0 GeV/c and $0.08 \le -t \le 0.20$ (GeV/c)^2 (Ref. 29) and where we have formed the difference of $\pi^- p \to \pi^+\pi^- n$ and $\pi^+ n \to \pi^+\pi^- p$ divided by the sum.

$$\rho_-^H \frac{d\sigma^{\pi N}}{dt\,dm}(s,t,m)=K|S_U^{\pi N}(s,t,m)|^2, \qquad (2.21b)$$

$$\rho_{00}^H \frac{d\sigma^{\pi N}}{dt\,dm}(s,t,m)=K|S_0^{\pi N}(s,t,m)|^2. \qquad (2.21c)$$

Each observable must be considered individually; if the corresponding β is $\approx -90°$ (90°) there will be a peak (dip) in that observable at the ω^0 mass.

One can understand the predictions shown in Fig. 28 by studying the relative ρ^0/ω^0 amplitude phases (β) resulting from these models. Figure 29 shows the relative phases $\beta_N^{\pi^- p}$, $\beta_U^{\pi^- p}$, and $\beta_0^{\pi^- p}$ for models 1a and 1b at 4.0 GeV/c for $t - t_0 = -0.1$ (GeV/c)^2. Both models have the same ρ^0 production amplitudes, which are also shown in Fig. 7. The ω^0 production amplitudes are quite different. Model 1a has the ρ and B poles contributing in phase to the amplitude $H^{n=0}_{-1;+}(\pi^- p \to \omega^0 n)$ (case 2, Fig. 19), which results in the negative and approximately real amplitude shown in Fig. 22. This results in the value of β_N of approximately −67°, shown in Fig. 29. By the use of (2.20a), (2.19a), and (2.21a) this results in a peaking at the ω^0 mass of the observable $\rho_+^H d\sigma/dt\,dm\,[\pi^- p \to (\pi^+\pi^-)n]$. Model 1b, on the other hand, has the ρ and B pole out of phase in $H^{n=0}_{-1-;+}(\pi^- p \to \omega^0 n)$ (case 1, Fig. 19), which results in the amplitude $H_f^N(\pi^- p \to \omega^0 n)$ being in the first quadrant (Fig. 22) and $\beta_N \approx 135°$ (Fig. 29). This model then predicts a dip at the ω^0 mass for the observable $\rho_+^H d\sigma/dt\,dm[\pi^- p \to (\pi^+\pi^-)n]$ as seen in Fig. 28.

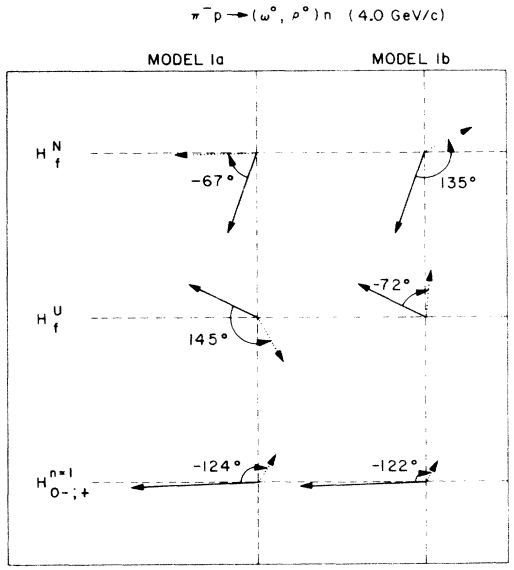

FIG. 29. Argand diagram showing the relative ρ^0 (solid arrows) and ω^0 (dotted arrows) production phases at 4.0 GeV/c and $t - t_0 = -0.1$ (GeV/c)^2 for models 1a and 1b. The ρ^0 (ω^0) production amplitudes were taken from Fig. 7 (Fig. 22).

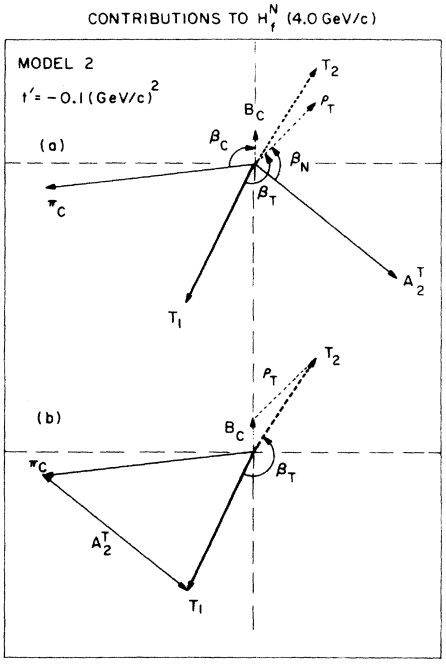

FIG. 30. (a) Argand diagram of the contributions to the amplitude $H_f^N (H_f^N = H_{1-;+}^{\eta=2} + H_{1-;+}^{\eta=0})$ for ρ^0 (solid arrows) and ω^0 (dashed arrows) production at 4.0 GeV/c and $t' \equiv t - t_0 = -0.1$ (GeV/c)^2 for model 2, where $\rho_T = \rho + \rho_C$ and $A_2^T = A_2 + A_2^C$. The total amplitude (pole + cut) for ρ^0 (ω^0) production is labeled T_1 (T_2). (b) Shows how the A_2 contribution (A_2^T) rotates the π-cut contributions (π_C) counterclockwise to a total value for ρ^0 production (T_1) and how the ρ contribution rotates the B-cut contribution (B_C) clockwise to a total value for ω^0 production (T_2). The resulting ω^0/ρ^0 relative phase is β_T.

The reason for the predicted behavior of $\rho_-^H\, d\sigma/dt\,dm$ seen in Fig. 28 can be traced through in a similar manner. Models 1b and 2 predict peaks in this observable for $\pi^- p \to \pi^+ \pi^- n$, whereas model 1a predicts a dip. All models predict peaks at the ω^0 mass for the observable $\rho_{00}^H d\sigma/dt\,dm(\,^-p \to (\pi^+\pi^-)n)$.

The predicted behavior of $\rho_+^H\, d\sigma/dt\,dm$ from models 1b and 2 is somewhat disturbing since these models are more successful in fitting the ω^0 production data than is model 1a. They are also more successful at predicting the behavior $\overline{K}^{*0}$ and K^{*0} production (discussed in Sec. IID). It is, therefore, important to understand precisely how the predicted behavior of $\rho_+^H\, d\sigma/dt\,dm$ arises in order to ascertain how firm this prediction is. Figure 30 shows the contributions to the ρ^0 and ω^0 production amplitude H_f^N at 4.0 GeV/c and $t - t_0 = -0.1$ (GeV/c)^2 resulting from model 2. We notice that if there were no ρ or A_2 pole contributions (only π cut and B cut), then $\beta = \beta_c$ would be approximately $-90°$. The π and B poles are $\approx -90°$ out of phase (Fig. 3) and, since the cuts are approximately 180° out of phase with the respective poles, the cuts are also approximately $-90°$ out of phase. Figure 31 shows that the π- and B-cut contributions to H_N^f do produce a spike in the observable $\rho_+^H\, d\sigma/dt\,dm$ at the ω^0 mass. The ρ and A_2 pole contributions for model 2 (and model 1b) have the EXD predicted phase (case 2, Fig. 19) and thus produce a $\beta = \beta_N = 90°$ resulting in a dip at the ω^0 mass for $\rho_+^H\, d\sigma/dt\,dm(\pi^- p \to \pi^+\pi^- n)$ (Fig. 31).[24] Figure 30(b) shows how the A_2 contribution to ρ^0 production rotates the π-cut contribution counterclockwise to from the total amplitude T_1. Similarly, this figure shows how the ρ contribution to ω^0 production rotates the B-cut contribution clockwise to total amplitude T_2. The resulting β_T is $\approx 180°$ and produces the behavior seen in Fig. 31 for the observable $\Delta\rho_+^H\, d\sigma/dt\,dm$ defined by (2.18).

It is clear that if the ρ and A_2 pole contributions to ρ_+ for ω^0 and ρ^0, respectively, are small enough and the absorption very large, then the total β for the amplitude H_f^N will be close to that for the π and B cuts ($\beta \approx \beta_c$), and the observable predicted $\rho_+^H\, d\sigma/dt\,dm(\pi^- p \to \pi^+\pi^- n)$ would peak at the ω^0 mass. It is not an easy matter, however, to reduce the amount of A_2 exchange in ρ^0 produc-

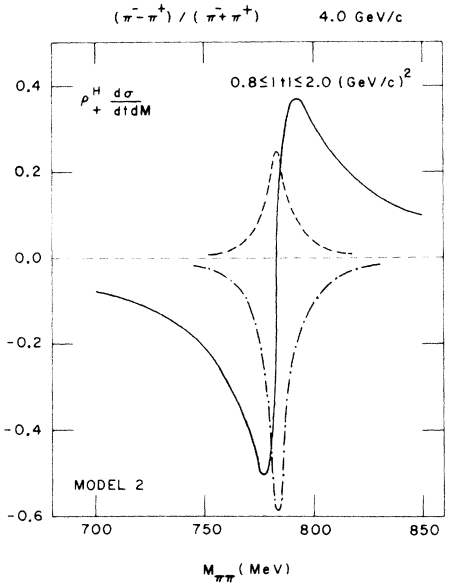

FIG. 31. The predicted ρ-ω interference behavior of the observable $\rho_+^H d\sigma/dt\,dm(\pi N \to \pi\pi N)$ at 4.0 GeV/c and $0.8 \le |t| \le 2.0$ (GeV/c)^2, where we have formed the difference between $\pi^- p \to \pi^+\pi^- n$ and $\pi^+ n \to \pi^+\pi^- p$ and divided by the sum. The dashed curve corresponds to the contributions arising from π and B cut alone in Fig. 30 (no ρ and A_2 pole; $\beta = \beta_C$). The dot-dashed curve is the contribution arising from the ρ and A_2 poles alone in Fig. 30 (no absorption; $\beta = \beta_N$) and the solid curve is the total contribution in Fig. 30 (pole + cut; $\beta = \beta_T$).

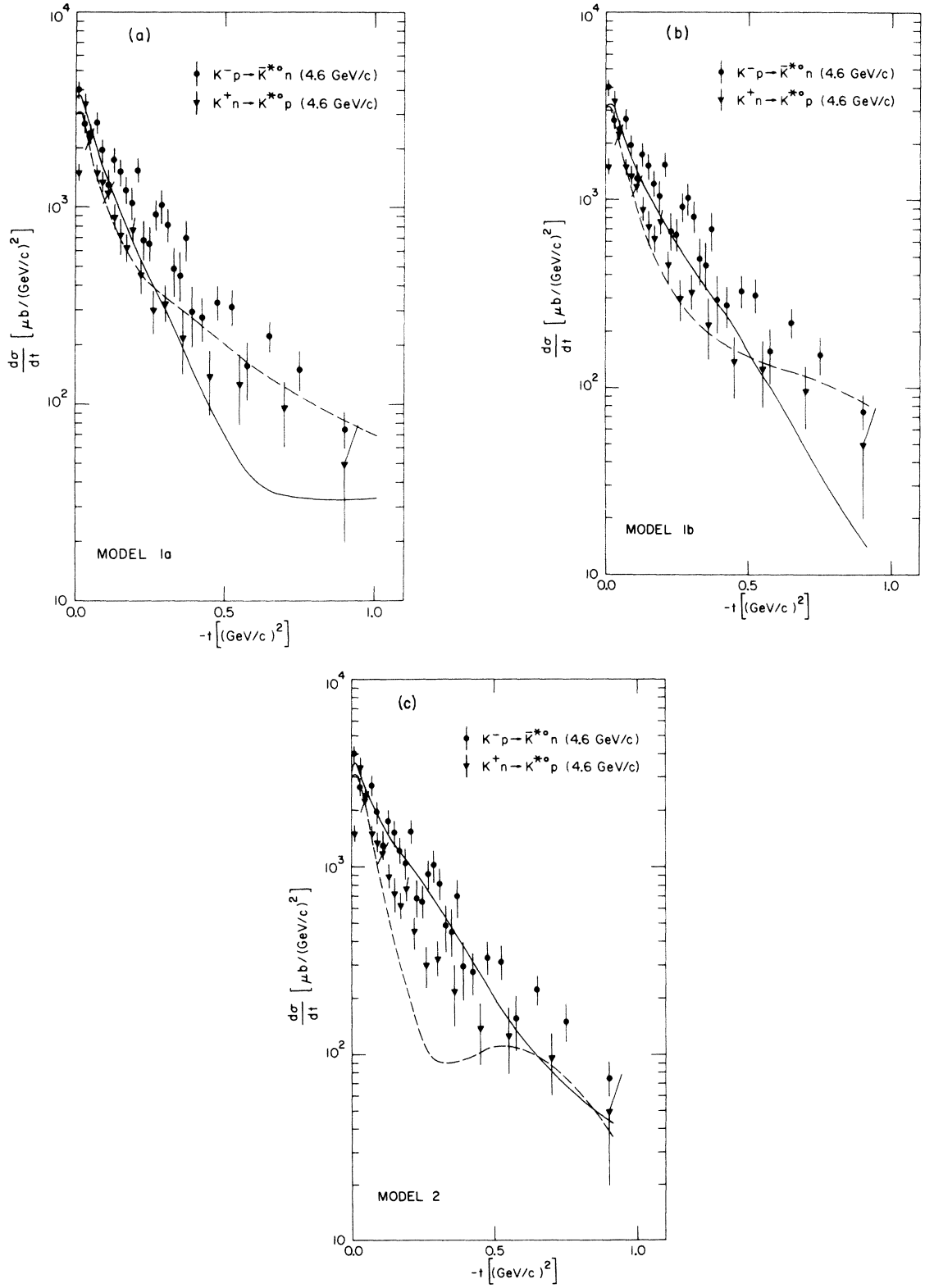

FIG. 32. Comparison of the data on the differential cross section for $K^-p \to \bar{K}^{*0}n$ (Ref. 41) and for $K^+n \to K^{*0}p$ (Ref. 42) at 4.6 GeV/c with the predictions of (a) model 1a, (b) model 1b, and (c) model 2. The solid (dashed) curves are the predicted values for $\bar{K}^{*0}$ (K^{*0}) production.

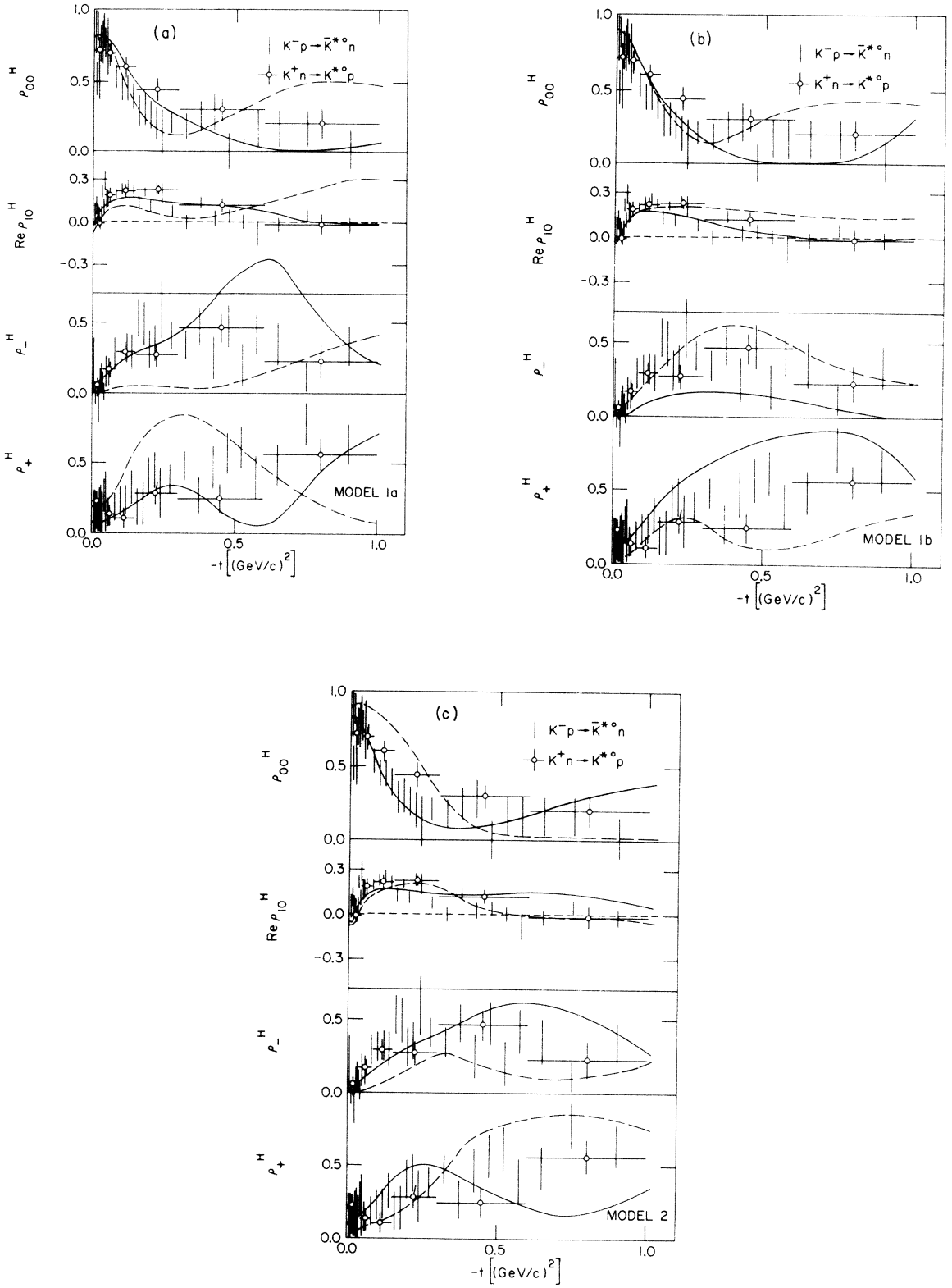

FIG. 33. Comparison of the data on the vector-meson density-matrix elements for $K^-p \to \bar{K}^{*0}n$ (Ref. 41) and $K^+n \to K^{*0}p$ (Ref. 42) at GeV/c with the predictions of (a) model 1a, (b) model 1b, and (c) model 2. The solid (dashed) curves are the predicted values for $\bar{K}^{*0}$ (K^{*0}) production.

tion for the following reasons:

(i) The A_2 cut helps in producing the desired small-$|t|$ spike in $\rho^H_{11}\, d\sigma/dt(\pi^- p \to \rho^0 n)$ (see Sec. II A 2).

(ii) A substantial amount of A_2 exchange is needed to fit the observed energy dependence of $\rho^H_+\, d\sigma/dt(\pi^- p \to \rho^0 n)$ (see Sec. II A 7). Even with no A_2 contribution to ρ^0 production the ρ contribution to ω^0 production will change β to a value quite a bit larger than $-90°$ [see Fig. 30(b)], and ρ exchange is needed to fit the small-$|t|$ behavior of $d\sigma/dt(\pi N \to \omega^0 N)$ (see Fig. 23).

The situation is similar for model 1b except that this model has less absorption than model 2 and a larger amount of ρ-pole contribution to ω^0 production (Fig. 23). This results in a β_T for the amplitudes H^N_f which is even closer to the pole prediction of $\approx 90°$ (see Fig. 24 and Fig. 29).

It is very important to learn the energy dependences of the ρ-ω interference effects shown in Fig. 27 at 4.0 GeV/c. Model 1a predicts that the spike at the ω^0 mass seen in $\rho^H_+\, d\sigma/dt\,dm(\pi^- p \to \pi^+\pi^- n)$ at 4.0 GeV/c will remain at all energies. If the spike changes to a dip at high energy ($\gtrsim$ 10 GeV/c) as predicted by models 1b and 2, then the discrepancies seen in Fig. 28 between the predictions of these two models and $\rho^H_+\, d\sigma/dt\,dm$ can be attributed to lower-lying effects (i.e., Regge-Regge cuts, daughters, etc.).[25]

D. Reactions $K^- p \to \bar{K}^{*0} n$ and $K^+ n \to K^{*0} p$

1. SU(3) predictions

From Table I it can be seen that given the strengths of the Regge exchanges for $\pi^- p \to \rho^0 n$ (π, A_2, and possibly A_1) and the Regge exchanges for $\pi^- p \to \omega^0 n(\rho, B)$, one can predict using SU(3) the strengths of the Regge exchanges for $K^- p \to \bar{K}^{*0} n$ and $K^+ n \to K^{*0} p(\pi,\ B,\ \rho,\ A_2$, and possibly A_1). If one further assumes that the s-channel helicity amplitudes for K^{*0} and $\bar{K}^{*0}$ production are absorbed in the same manner as corresponding amplitudes for ρ^0 and ω^0 production, then the total amplitudes for K^{*0} and $\bar{K}^{*0}$ production can be *predicted* from the Regge amplitudes determined in Sec. II A and Sec. II B. In Figs. 32(a), 32(b), and 32(c) we compare the data on the differential cross sections for $K^- p \to \bar{K}^{*0} n$ and $K^+ n \to K^{*0} p$ at 4.6 GeV/c with the predictions of models 1a, 1b, and 2, respectively. In Figs. 33(a), 33(b), and 33(c) the vector-meson density-matrix elements for K^{*0} and $\bar{K}^{*0}$ production are compared with the predictions of models 1a, 1b, and 2, respectively. We see that models 1b and 2 are able to give a good description of the K^{*0} and $\bar{K}^{*0}$ data, whereas model 1a is not.

2. Line-reversal behavior

In the absence of absorption and with EXD trajectories [$\alpha_\rho(t) = \alpha_{A_2}(t)$, $\alpha_\pi(t) = \alpha_B(t)$] the differential cross sections for $K^- p \to \bar{K}^{*0} n$ and its line-reversal partner $K^+ n \to K^{*0} p$ are predicted to be equal. The data (Fig. 32) show that the two cross sections agree roughly in the forward direction, but away from the forward direction the cross section for K^{*0} production is steeper and lies below the one for $\bar{K}^{*0}$ production.[26] As can be seen, this behavior is predicted from models 1b and 2. It is of interest to examine in detail how this line-reversal breaking is produced in these models.[27]

The line-reversal breaking predicted in the differential cross sections for K^{*0} and $\bar{K}^{*0}$ from models 1b and 2 comes primarily from the amplitude H^N_f [(2.8a)]. In Fig. 34 we present an Argand diagram of the contributions to this amplitude for $\bar{K}^{*0}$ and K^{*0} production at 4.6 GeV/c and $t - t_0 = -0.2$ (GeV/c)^2 resulting from model 1b. The amplitude H^N_f for $\bar{K}^{*0}$ and K^{*0} receives contributions from the π cut by the same mechanism as in ρ^0 production (see Sec. II A 6). This amplitude thus receives contributions from the ρ, ρ cut, A_2, A_2 cut, and the π cut (also small contributions from the B cut). The ρ and ρ-cut contributions change sign under line reversal, while the A_2, A_2-cut, and π-cut contributions do not (see Table I). Thus symbolically we have

$$|H^N_f(\bar{K}^{*0})|^2 - |H^N_f(K^{*0})|^2 \propto 2\,\mathrm{Re}(\rho A_2^*) + 2\,\mathrm{Re}(\rho A_2^{C*}) + 2\,\mathrm{Re}(\rho\pi_C^*) + 2\,\mathrm{Re}(\rho_C A_2^*) + 2\,\mathrm{Re}(\rho_C A_2^{C*}) + 2\,\mathrm{Re}(\rho_C \pi_C^*). \quad (2.22)$$

From Fig. 34 it can be seen that the main contribution to (2.22) comes from the term $\mathrm{Re}(\rho\pi_C^*)$, but there are also important contributions from $\mathrm{Re}(\rho A_2^{C*})$. Figure 34 shows that, although the pole contributions to K^{*0} and $\bar{K}^{*0}$ production are about equal under line reversal (actually model 1b has the pole contribution to K^{*0} slightly larger than that for $\bar{K}^{*0}$ production), the cut corrections are larger for K^{*0} production, producing a smaller total amplitude for this reaction.[28]

It should also be pointed out that, although model 1b abandons EXD of the Regge poles, Fig. 34 shows that the resulting total amplitude (pole + cut) H^N_f for K^{*0} is almost purely real (for small $|t|$), whereas the total amplitude for $\bar{K}^{*0}$ production has a large imaginary part. This is precisely what one would expect from a model with EXD Regge poles and no absorption.

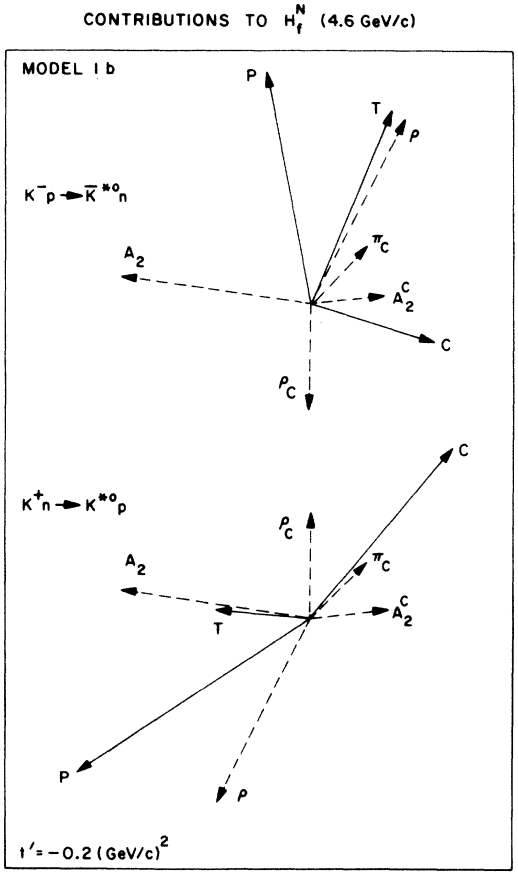

FIG. 34. Argand diagram of the contributions to the s-channel helicity amplitude H_f^N ($H_f^N = H_{1-;+}^{n=2} + H_{-1-;+}^{n=0}$) for $\bar{K}^{*0}$ and K^{*0} production at 4.6 GeV/c and $t' \equiv t - t_0 = -0.2$ (GeV/c)^2 from model 1b. The labels P and C correspond to the total pole ($A_2 + \rho$) and total cut ($\pi_C + A_2^C + \rho_C$) contributions, respectively. The total amplitude (pole + cut) is labeled by T.

3. *Unmeasured observables: A_1 exchange?*

The polarized target asymmetry observables A_N^1, A_u^1, A_u^0, and A [(2.5) and (2.7)] and the recoil nucleon polarization P_r [(2.6)] can be used just as in ρ^0 production to test for the presence of A_1 exchange in $\bar{K}^{*0}$ and K^{*0} production. Figure 14 shows the predicted values of these observables for $\bar{K}^{*0}$ production at 4.6 GeV/c using model 1b (no A_1 exchange) and model 3 (A_1 exchange). It can be seen that for model 1b $A_u^1 = A_u^0 = 0$ and $P_r = A$, but for model 2 A_u^1 and A_u^0 are not zero and $P_r \neq A$.

III. SUMMARY AND CONCLUSIONS

We have applied several Regge-pole absorption models and SU(3) to the six charge-exchange vector-meson production reactions (1.1)-(1.6). We have placed particular emphasis on the behavior of the production amplitudes resulting from these models. We summarize the models, their successes, and possible trouble spots as follows:

Model 1. This model, introduced by Hartley and Kane[5] in their work on pseudoscalar production, uses a fancy Pomeron type of absorption and non-EXD-type Regge signature factors (with no WSNZ for the ρ trajectory). The model absorbs all production amplitudes in a similar manner. Model 1b uses the EXD predicted phase relationship for the ρ and A_2, whereas model 1a has the opposite ρ-A_2 relative phase. Model 1b does an excellent job of describing the low-energy observables (differential cross section and vector-meson density-matrix elements) for ρ^0 and ω^0 production and successfully predicts the observables for $\bar{K}^{*0}$ and K^{*0} production including the proper line-reversal breaking. This model correctly predicts the energy dependence of $d\sigma/dt(\pi^- p \to \rho^0 n)$, but has troubles with the energy dependence of $\rho_{00}^H\, d\sigma/dt$ (predicts more shrinkage than observed) and $\rho_{+}^H\, d\sigma/dt$ (predicts too much of a decrease with energy). Model 1b also has problems predicting the observed ρ-ω interference effects at 4.0 GeV/c in the observable $\rho_{+}^H\, d\sigma/dt\,dm(\pi N \to \pi\pi N)$. Model 1a, on the other hand, predicts the correct behavior of $\rho_{+}^H\, d\sigma/dt\,dm(\pi N \to \pi\pi N)$ at 4.0 GeV/c but has trouble in fitting the behavior of $\mathrm{Re}\rho_{10}^H$ for ω^0 production and does not give good predictions for K^{*0} and $\bar{K}^{*0}$ production. We feel that model 1b has the correct ρ-A_2 pole phase relation and that its inability to predict correctly the ρ-ω interference effects in $\rho_{+}^H\, d\sigma/dt\,dm(\pi N \to \pi\pi N)$ at 4.0 GeV/c lies elsewhere (lower-lying exchanges, Regge-Regge cuts, etc.). We feel that higher-energy experiments ($\gtrsim$8 GeV/c) will exhibit ρ-ω interference effects similar to those predicted by model 1b [dip rather than peak in mass spectra $\rho_{+}^H\, d\sigma/dt\,dm(\pi^- p \to \pi^+\pi^- m)$ at the ω^0 mass[25]].

Model 2. This model is a generalization of the square-cut absorption model used by Worden in his work on photoproduction.[11] In this model each net helicity-flip amplitude is absorbed differently; large square-cut absorption for $n = 0$ amplitudes, less absorption (still large) for $n = 1$ amplitudes, and no absorption for $n = 2$ amplitudes. This model uses EXD-type Regge signature factors (with a WSNZ for the ρ trajectory). The predictions of this model are very similar to those of model 1b. It does well in explaining the behavior of the low-energy observables (differential cross sections and vector-meson density-matrix elements) for ρ^0 and ω^0 production and successfully predicts the behavior of K^{*0} and $\bar{K}^{*0}$ production. It has difficulties with the energy dependences of $\rho_{00}^H\, d\sigma/dr$ and $\rho_{+}^H\, d\sigma/dt$ for ρ^0 production and does not correctly predict the ρ-ω interference effects seen at

4.0 GeV/c in the $\pi\pi$ mass spectra projection $\rho^H_+ d\sigma/dt\,dm(\pi N \to \pi\pi N)$.

It is difficult to distinguish experimentally between models 1b and 2. One possible area of distinction is in the small-$|t|$ energy dependence of $\rho^H_{11} d\sigma/dt$ for ρ^0 production. The small-$|t|$ behavior of $\rho^H_{11} d\sigma/dt$ is given primarily by the π cut, and the two models predict quite different energy dependences for the cuts (see Fig. 17). Model 1b appears to do a better job at fitting the experimentally observed energy dependence (see Fig. 9).

Model 3. This model is identical to model 2 except that it has *only* $n=0$ absorption and includes a large A_1 contribution. This model can be tested experimentally by measuring the polarized target asymmetry observables [A^0_u, A^1_u, and A; see (2.5)] and the recoil-nucleon polarization P_r (2.6). Models without A_1 exchange predict $A^0_u = A^1_u = 0$ and $A = P_r$, whereas models with A_1 exchange have $A^0_u \neq 0$ and/or $A^1_u \neq 0$ and $A \neq P_r$.

Throughout this paper we have made many predictions using various Regge-pole absorption models, and we feel that the following are useful areas of experimental investigation.

1. The statistics for ω^0 production should be greatly improved, allowing for the observation of ρ-ω mixing effects. In particular it would be nice to verify the predicted isospin violation occurring in $\rho^H_{00} d\sigma/dt(\pi N \to \omega N)$ (see Fig. 26).

2. The statistics for K^{*0} and $\bar{K}^{*0}$ production should be improved to allow for a better test of the line-reversal breaking predicted in Fig. 32. Also, it is of great interest to study the energy dependence of the line-reversal breaking.

3. Another high-energy (> 17 GeV/c) ρ^0 production experiment should be performed to check the apparent lack of shrinkage of $\rho^H_{00} d\sigma/dt$. This lack of shrinkage is disastrous for models that consider the π as a Regge pole.

4. As we have seen ρ-ω mixing effects provide valuable information about the nature of the ρ^0 and ω^0 strong-interaction production amplitudes. Further experimental studies of the observables $\rho^H_{00} d\sigma/dt\,dm$ and $\rho^H_+ d\sigma/dt\,dm$ for $\pi N \to \pi\pi N$ would be very useful especially at higher energies ($\gtrsim$ 8 GeV/c). It would be extremely interesting to know the energy dependence of the ρ-ω interference effects shown in Fig. 27. Does the peaking observed at 4.0 GeV/c in the quantity $\rho^H_+ d\sigma/dt\,dm(\pi^- p \to \pi^+\pi^- n)$ become a dip at higher energies as predicted by models 1b and 2?[25]

5. The experiments with the most impact would be measurements of the as yet unobserved polarized target asymmetries A^1_N, A^0_N, A^1_u, and A [see (2.5) and (2.6)] and the measurements of the recoil-nucleon polarization P_r for ρ^0, ω^0, K^{*0}, and $\bar{K}^{*0}$ production. These types of experiments would settle the question of how important is A_1 exchange in ρ^0, K^{*0}, and $\bar{K}^{*0}$ production (see Fig. 14).

ACKNOWLEDGMENTS

We acknowledge useful discussions with Dr. G. Kane, Dr. C. Quigg, and Dr. G. Fox. We thank Dr. C. B. Chiu for his participation during the early stages of this work. We are very grateful to the following experimenters for interesting discussions and for allowing us access to their data: R. Diebold, D. Ayres, A. Greene, S. Kramer, A. Pawlicki, and A. Wicklund at Argonne; H. Gordon, K.-W. Lai, and J. M. Scarr at Brookhaven National Laboratory; S. Barish and W. Selove at Argonne. Finally, we thank Dr. R. F. Peierls for his support during the course of this work.

---

*Work performed, in part, under the auspices of the U. S. Atomic Energy Commission, and, in part, by National Science Foundation Grant No. P032998X1.

†Present address: Lauritsen Laboratory of High Energy Physics, California Institute of Technology, Pasadena, Calif. 91109.

‡Present address: Department of Physics, Rutgers—The State University, New Brunswick, N. J. 08903.

[1]For a review of this subject see, for example, G. C. Fox and C. Quigg, Annu. Rev. Nucl. Sci. 23, 219 (1973); R. D. Field, in π-π *Scattering—1973,* proceedings of the international conference on π-π scattering and associated topics, Tallahassee, 1973, edited by P. K. Williams and V. Hagopian (A.I.P., New York, 1973).

[2]F. Halzen and C. Michael, Phys. Lett. 36B, 367 (1971).

[3]Also see R. Kelly, Phys. Lett. 39B, 635 (1972).

[4]C. B. Chiu, in *Proceedings of the Workshop on Particle Physics at Intermediate Energies,* edited by R. D. Field (Lawrence Berkeley Laboratory, Berkeley, Calif., 1971).

[5]B. J. Hartley and G. L. Kane, Nucl. Phys. B57, 157 (1973).

[6]For a further discussion of these reactions including additional model fits not exhibited in this paper, see Deepinder Sidhu, Ph.D. thesis, Institute for Theoretical Physics, State University of New York at Stony Brook, Stony Brook, New York, 1973 (unpublished); R. D. Field and Deepinder P. Sidhu, Brookhaven National Laboratory Report No. BNL 18181, 1973 (unpublished).

[7]Obviously the assumptions used to derive (1.7a) and (1.7b) cannot hold exactly since they predict $d\sigma/dt(\bar{K}^{*0}n) = d\sigma/dt(K^{*0}p)$, which does not hold for $P_{\rm lab} < 10$ GeV/c.

[8]The parametrizations for $P(s,t)$ and $D_0(s,t)$ are taken directly from the values determined by Hart-

ley and Kane in their fits to pseudoscalar production ($PB \to P'B'$, Ref. 5) except for the over-all strength of the diffractive piece (d_0) which we found necessary to increase from the value of 50 used by Hartley and Kane to a value of ≈80. This results in larger absorption for vector-meson production than for pseudoscalar production.

[9]The total helicity partial-wave amplitudes are given by multiplying the corresponding Regge partial-wave amplitudes by $f^j_{\text{eff}}(s)$.

[10]All residues are s-channel residues. See Ref. 6 for details of the parametrizations and resulting parameters.

[11]R. Worden, Nucl. Phys. B37, 253 (1972).

[12]The quantity K is given by $K = 1/128\pi s p_s^{\,2}$.

[13]See, for example, Lorella Jones, Phys. Rev. 163, 1523 (1967).

[14]The Williams model (or "poor man's absorption model") also predicts this behavior. We have not discussed this model since we feel that it is more a model of pion-pole extrapolation than a generalized absorption model. For a discussion of this model we refer the reader to G. Fox, invited talk at Argonne Workshop on Meson Spectroscopy, August 1971 (unpublished) and the references therein.

[15]See, for example, E. L. Berger and G. C. Fox, Phys. Rev. Lett. 25, 1783 (1970).

[16]Some of these expectations are discussed by G. L. Kane, in *Experimental Meson Spectroscopy*, edited by C. Baltay and A. H. Rosenfeld (Columbia Univ. Press, New York, 1970).

[17]See, also, the discussions by Geoffrey Fox, invited talk at the Second International Conference on Polarization and Polarized Targets, Berkeley, 1971 (unpublished).

[18]This section was inspired by a set of notes on the subject by G. Kane and A. Martin (unpublished).

[19]For a review see Matts Roos, talk given at the Daresbury Study Weekend, June, 1970, on Vector-Meson Production and Omega-Rho Interference (unpublished); Gerson Goldhaber, in *Experimental Meson Spectroscopy*, edited by C. Baltay and A. H. Rosenfeld (Columbia Univ. Press, New York, 1970).

[20]S. Coleman and S. Glashow, Phys. Rev. Lett. 6, 423 (1961); Phys. Rev. 134, B671 (1964); S. L. Glashow, Phys. Rev. Lett. 7, 469 (1961); S. Coleman and H. J. Schnitzer, Phys. Rev. 136, B223 (1964); R. Socolow, Phys. Rev. 137, B1221 (1965).

[21]J. Lefrançois, in *Proceedings of the 1971 International Symposium on Electron and Photon Interactions at High Energies*, edited by N. B. Mistry (Laboratory of Nuclear Studies, Cornell University, Ithaca, N.Y., 1972).

[22]A. S. Goldhaber, G. C. Fox, and C. Quigg, Phys. Lett. 30B, 249 (1969).

[23]N. N. Achasov and G. N. Shestakov, Nucl. Phys. B45, 93 (1972).

[24]C. Quigg, Univ. of California at Berkeley Report No. UCID-3413 (unpublished).

[25]Recent ρ-ω interference data for $\pi^- p \to \pi^+\pi^- n$ at 17.2 GeV/c do indicate that the spike seen at the ω^0 mass in $\rho^H_+\, d\sigma/dt\, dm$ at 4.0 GeV/c has indeed changed to a dip, in agreement with models 1b and 2 (A. Martin, private communication).

[26]For a review of K^{*0} and $\bar{K}^{*0}$ production see R. L. Eisner, talk presented at International Winter meeting on Fundamental Physics, Formigal, Spain, February, 1973 (unpublished).

[27]See also the model fits and discussions of K^{*0} and $\bar{K}^{*0}$ production presented by G. C. Fox, R. Engelmann, B. Musgrave, F. Schweingruber, H. Yuta, B. Forman, N. Gelfand, and H. Schulz, Phys. Rev. D 4, 2627 (1971).

[28]The suggestion that the ρ pole and π cut might be responsible for line-reversal differences was made by G. Kane in Ref. 24.

[29]D. S. Ayres, R. Diebold, A. F. Greene, S. L. Kramer, A. J. Pawlicki, and A. B. Wicklund, contributed paper presented by S. L. Kramer at the International Conference on π-π Scattering and Associated Topics, Tallahassee, 1973 (unpublished.

[30]S. Barish and W. Selove, private communication.

[31]H. Gordon, K.-W. Lai, and J. M. Scarr, Phys. Rev. D 8, 779 (1973).

[32]F. Bulos, R. K. Carnegie, G. E. Fisher, E. E. Kluge, D. W. G. S. Leith, H. L. Lynch, B. Ratcliff, B. Richter, H. H. Williams, S. H. Williams, and M. Beniston, Phys. Rev. Lett. 26, 1453 (1971).

[33]D. S. Ayres, R. Diebold, A. F. Greene, S. L. Kramer, A. J. Pawlicki, and A. B. Wicklund, invited paper presented by R. Diebold at the International Conference on π-π Scattering and Associated Topics, Tallahassee, 1973 (unpublished.

[34]J. A. J. Matthews, J. D. Prentice, T. S. Yoon, J. T. Carroll, M. W. Firebaugh, and W. D. Walker, Nucl. Phys. B (to be published).

[35]The CERN-Munich 17.2-GeV/c $\pi^- p \to \rho^0 n$ data were arrived at by calculating the observables from the amplitude analysis of P. Estabrooks and A. D. Martin, in *Experiments on High Energy Particle Collisions—1973*, proceedings of the international conference on new results from experiments on high energy particle collisions, Vanderbilt University, 1973, edited by Robert S. Panvini (A.I.P., New York, 1973), p. 357.

[36]The 17.2-GeV/c CERN-Munich data were normalized such as to produce an effective α of zero at $t = 0$ for $\rho^H_{00}\, d\sigma/dt$.

[37]L. E. Holloway, B. Huld, M. Jordan, D. W. Mortara, E. I. Rosenberg, A. D. Russell, S. Bernstein, M. H. Garrell, S. Margulies, and D. W. Mcleod, Phys. Rev. Lett. 27, 1671 (1971).

[38]J. A. J. Matthews, J. D. Prentice, T. S. Yoon, J. T. Carroll, M. W. Firebaugh, and W. D. Walker, Phys. Rev. Lett. 26, 400 (1971).

[39]J. C. Anderson, A. Engler, R. W. Kraemer, S. Toaff, F. Weisser, J. Diaz, F. DiBianca, W. Fickinger, and D. K. Robinson, report (unpublished).

[40]The first two bins of the 6.0-GeV/c $\pi^+ n \to \omega^0 p$ data (Ref. 39) violate the spin-one positivity condition that requires $0 \le \rho_- \le 1$ (the data have ρ_- negative in the first two bins). The extremely large values of ρ_{00} for these two bins is therefore probably misleading.

[41]M. Aguilar-Benitez, R. L. Eisner, and J. B. Kinson, Phys. Rev. D 4, 2583 (1971).

[42]K. Buchner, G. Dehm, W. Geist, G. Göbel, W. Wittek, G. Wolf, G. Charrière, W. Dunwoodie, Y. Goldschmidt-Clermont, A. Grant, U. P. Henri, F. Muller, J. Quinguard, Z. Sekera, P. Cornet, G. De Jongh, P. Dufour, F. Grard, J. Milkin, S. Tavenier, and R. Windmolders, Nucl. Phys. B45, 333 (1972).